NOVA SCHOOL OF SCIENCE & TECHNOLOGY

DEPARTMENT OF CHEMISTRY

GUILHERME FRADINHO FERNANDES MALVEIRO

BSc in Chemical and Biological engineering

DEVELOPMENT AND ELECTROCHEMICAL TESTING OF A NEW FAMILY OF ELECTRODES FOR SOLID OXIDE CELLS

THE FUTURE OF ENERGY PRODUCTION

MASTER IN CHEMICAL AND BIOLOGICAL ENGINEERING

NOVA University Lisbon
September, 2025

NOVA SCHOOL OF SCIENCE & TECHNOLOGY

DEPARTMENT OF CHEMISTRY

DEVELOPMENT AND ELECTROCHEMICAL TESTING OF A NEW FAMILY OF ELECTRODES FOR SOLID OXIDE CELLS

THE FUTURE OF ENERGY PRODUCTION

GUILHERME FRADINHO FERNANDES MALVEIRO

BSc in Chemical and Biological engineering

Adviser: Antonio Maria
Supervisor, Institut de Recerca en Energia de Catalunya

Co-adviser: Ana Maria Staack Reis Machado
Researcher, NOVA School of Science and Technology

Examination Committee

Chair: Name of the committee chairperson
Full Professor, FCT-NOVA

Rapporteur: Name of a rapporteur
Associate Professor, Another University

Members: Another member of the committee
Full Professor, Another University

Yet another member of the committee
Assistant Professor, Another University

MASTER IN CHEMICAL AND BIOLOGICAL ENGINEERING

NOVA University Lisbon
September, 2025

Development and electrochemical testing of a new family of electrodes for Solid Oxide Cells

The future of energy production

For my family and friends.
Thank you for everything.

Acknowledgements

Gostaria de expressar a minha profunda gratidão a todos que tornaram este trabalho possível. Em primeiro lugar, agradeço aos meus dois supervisores Antonio Maria e Kosova Kreka e aos meus orientadores Mário Eusébio e Ana Machado pela orientação, apoio e paciência ao longo deste percurso. Agradeço também à instiutuição IREC e à minha universidade NOVA-SST por tornar o meu estágio e tese possiveis em Barcelona. Agradeço também à minha família e amigos pelo incentivo constante e compreensão nos momentos mais desafiantes. Por fim, agradeço a todas as pessoas que, de alguma forma, contribuíram para a realização desta tese.

This work received funding from FCT (Fundação para a Ciência e Tecnologia, I.P.) under the projects LA/P/0008/2020 DOI 10.54499/LA/P/0008/2020; UIDP/50006/2020 DOI 10.54499/UIDP/50006/2020; UIDB/50006/2020 DOI 10.54499/UIDB/50006/2020 of the Associate Laboratory of Green Chemistry and projects of LA/P/0037/2020, UIDP/50025/2020 and UIDB/50025/2020 of the Associate Laboratory Institute of Nanostructures, Nanomodelling and Nanofabrication – i3N, and by the project CO2RED (DOI 10.54499/PTDC/EQU-EPQ/2195/2021). The work was also supported by the project M-ECO2 – Industrial cluster for advanced biofuel production, Ref. C644930471-00000041, co-financed by PRR - Recovery and Resilience Plan of the European Union (Next Generation EU). The authors also acknowledge funding from the European Union via the projects X-STREAM (Horizon EU, ERC-2023- CoG, No. 101124803). Views and opinions expressed are, however, those of the authors only and do not necessarily reflect those of the European Union or the European Research Council. Neither the European Union nor the granting authority can be held responsible for them.

In this work, generative artificial intelligence tools, namely Chat GPT by OpenAI were used for grammatical review and text reformulation. These tools were employed under the author's supervision, and all generated content was checked for accuracy. The authorship and validation of the content remain entirely the responsibility of the author, and the use of artificial intelligence complies with institutional standards of academic integrity.

”

“O segredo do crescimento está na coragem de tentar e na humildade de aprender com cada passo.”

— **Fernando Pessoa**, Mensagem pessoal (Amigo)

Abstract

The exponential rise in population, urbanization, and industrialization, together with modern living standards, has led to a sharp increase in energy demand. Heavy reliance on fossil fuels has severely affected the environment and human health, with the power sector standing out as a major source of greenhouse gas emissions and pollutants. As a result, hydrogen has gained significant attention as a clean alternative, and many nations are investing in fuel cell research. Among these, solid oxide fuel cells (SOFCs) have emerged as a commercially viable option at small scale, producing negligible emissions and showing promise through efforts to reduce operating temperatures, material costs, and polarization losses. Within this context, High Entropy Oxides (HEOs), a class of High Entropy Materials (HEMs), have drawn increasing interest over the past 15 years due to their potential to enhance SOFC technology. To explore this potential, two types of HEOs were tested: HEO-5, containing chromium, and HEO-7, without chromium. They were subjected to electrochemical and morphological experiments to assess their behavior as electrodes. HEO-5 corresponded to expectations, maintaining a stable current over long periods and performing comparably to other electrodes. In solid oxide electrolysis cell (SOEC) mode, it showed a polarization resistance (Rp) of 0.207 $\Omega \cdot cm^2$ at 900°C, with cell voltage degrading only slightly from 1.080 V to 1.020 V after 72 h at 0.195 A/cm^2. In contrast, HEO-7 did not meet expectations, although the absence of chromium was thought to improve performance by avoiding cluster formation, its results were less favorable as it exhibited an Rp of 0.110 $\Omega \cdot cm^2$ at 900°C but degraded almost immediately under operation. Additionally, HEO-7 requires further optimization of its microstructure and electrode/electrolyte interface before its suitability for future research can be determined.

Keywords: SOFC, SOEC, High Entropy Oxides

Resumo

O aumento exponencial da população, urbanização e industrialização, aliado aos padrões de vida modernos, levou a um acentuado crescimento da procura de energia. A forte dependência dos combustíveis fósseis afetou gravemente o ambiente e a saúde humana, destacando-se o setor elétrico como uma das principais fontes de emissões de gases com efeito de estufa e poluentes. Como resultado, o hidrogénio tem ganho uma atenção significativa como alternativa limpa, e muitos países estão a investir em investigação sobre células de combustível. Entre estas, as células de combustível de óxido sólido (SOFCs) surgiram como uma opção comercialmente viável em pequena escala, produzindo emissões praticamente nulas e revelando potencial através de esforços para reduzir as temperaturas de operação, os custos dos materiais e as perdas por polarização. Neste contexto, os Óxidos de Alta Entropia (HEOs), uma classe de materiais de Alta Entropia (HEMs), têm despertado crescente interesse nos últimos 15 anos devido ao seu potencial para melhorar a tecnologia SOFC. Para explorar esse potencial, foram testados dois tipos de HEOs: HEO-5, contendo crómio, e HEO-7, sem crómio. Estes foram submetidos a ensaios eletroquímicos e morfológicos para avaliar o seu comportamento como eletrodos. O HEO-5 correspondeu às expectativas, mantendo uma corrente estável durante longos períodos e apresentando um desempenho comparável a outros eletrodos. Em modo de célula eletrolítica de óxido sólido (SOEC), apresentou uma resistência de polarização (Rp) de 0,207 $\Omega \cdot cm^2$ a 900 °C, com a tensão da célula a degradar apenas ligeiramente de 1,080 V para 1,020 V após 72 h a 0,195 A/cm^2. Em contraste, o HEO-7 não correspondeu às expectativas; embora se pensasse que a ausência de crómio pudesse melhorar o desempenho ao evitar a formação de aglomerados, os seus resultados foram menos favoráveis, exibindo uma Rp de 0,110 $\Omega \cdot cm^2$ a 900 °C mas degradando quase imediatamente em operação. Além disso, o HEO-7 requer uma otimização adicional da sua microestrutura e da interface eletrodo/eletrólito antes que a sua adequação para futuras investigações possa ser determinada.

Palavras-chave: SOFC, SOEC, Óxidos de Alta Entropia

Contents

List of Figures

List of Tables

Acronyms

ASR Area-Specific Resistance *20*, *26*, *27*, *32*, *33*, *37–39*, *41*, *42*)

BL Barrier Layer *6*)

CGO Ceria-Gadolinia *6*, *11*, *12*)

Ea Activation Energy *27*, *34*, *42*, *43*)
EDX Energy Dispersive X-ray *20*)
EIS Electrochemical Impedance Spectroscopy *17*, *18*, *20*, *23*, *25*, *29*, *31*, *33*, *37*, *40*, *44*, *45*)

FE Fuel Electrode *5*, *7*)

HEO High Entropy Oxide *1*, *3*, *8*, *9*, *11*, *14*, *18*, *21*, *36*)
HEO-5 High Entropy Oxide 5 *10*, *11*, *16–18*, *20–35*, *42*, *44*, *45*)
HEO-7 High Entropy Oxide 7 *10*, *12*, *17*, *18*, *20*, *36–42*, *44*, *45*)

LSCF Lanthanum strontium cobalt ferrite *4*, *37*)
LSM Lanthanum strontium manganite *4*, *39*)

MIEC Mixed ionic and electronic conductivity *4*)

NiO-YSZ Nickel oxide-yttria-stabilized zirconia *5*)

OE Oxygen Electrode *4*, *7*)
OER Oxygen Evolution Reaction *4*)
ORR Oxygen Reduction Reaction *4*)

PLD Pulsed Laser Deposition *6*)

Rp Polarization Resistance *20, 25–28, 31–35, 37–45)*
Rs Ohmic Resistance *20, 25–28, 31–35, 37–39, 41, 42)*

SED Secondary Electron Detector *20, 21)*
SEM Scanning electron microscope *16, 20, 22)*
SOC Solid Oxide Cell *2–4, 6–9)*
SOEC Solid Oxide Eletrolyzer Cell *2, 3, 10, 11, 17–20, 23–28, 37–39, 44, 45)*
SOFC Solid Oxide Fuel Cell *1, 3, 7–11, 17–21, 29–35, 40–42, 44, 45)*

XRD X-ray diffraction *14, 20, 36)*

YSZ Yttrium-Stabilized Zirconia *4)*

1 Introduction

1.1 Introduction

A global effort is being made by many countries for decarbonization in order to reshape energy systems targeting zero emissions by 2050. Challenges remain a huge problem such as performance, storage, and reliability as expanding renewable energy and accelerating electrification are essential to this transition. With this said, SOFCs present a real solution to those problems: high temperature devices that generate electricity directly from fuels such as hydrogen or natural gas. They use a solid ceramic electrolyte that conducts oxygen ions, with oxygen reduced at the cathode and fuel oxidized at the anode, delivering high efficiency along with a low emission energy conversion that can complement other renewable energy sources and promote a sustainable future. Despite their advantages, further improvements in SOFC performance, durability, and cost are still needed for large scale deployment. In particular, the development of advanced electrode materials is crucial for enhancing electrochemical activity and long term stability under demanding operating conditions. High Entropy Oxides (HEOs) have recently emerged as a promising class of materials for SOFC electrodes. Defined by their multi-component cationic configuration and high configurational entropy, HEOs can exhibit unique combinations of properties such as enhanced thermal stability, improved redox tolerance, and adaptable catalytic activity. Their ability to form stable single phase structures even with five or more metal species makes them attractive candidates for both fuel-electrode and air-electrode applications, opening new pathways to overcome limitations found in conventional perovskite or fluorite-based materials [1, 2].

1.2 Fundamentals of Operation of SOFC/SOEC

For energy production (SOFC mode), hydrogen is mainly used as the fuel: one electrode is first supplied with hydrogen, and the H_2 molecules interact with the electrode material, dissociating into H^+ ions in an oxidation reaction, where the electrode acts as a catalyst. The released electrons travel through an external circuit to be used for power, while the

ions migrate via a hopping mechanism through the electrolyte, making their way to the opposite electrode through the material's porous structure. Upon reaching the opposite electrode, the H^+ ions react with the oxygen present in the atmosphere, forming water after receiving the electrons previously released. This reduction reaction takes place within the electrode, which serves as a catalyst. In SOEC mode, this process is reversed, where a voltage is applied while (H_2O) steam is supplied, leading to its electrolysis into hydrogen and oxygen, enabling hydrogen production. These cells are stacked together using bipolar plates, where the positive pole of one cell is connected to the negative pole of the next. In other words, each electrode connects to the opposite electrode of the adjacent cell [3–7].

1.2.1 Operating temperatures

Solid Oxide Cells (SOCs) can also be categorized by analyzing the temperature operation range. They can be **high-temperature SOCs** (>850ºC), **intermediate-temperature SOCs** (650-850ºC), or **low-temperature SOCs** (400-650ºC). The higher the operating temperature, the higher the voltage produced and leakage probability, and therefore the smaller the lifespan [3, 8].

1.2.2 Polarization losses

Cell voltage losses can occur when electrons travel inside the cell and through the external circuit due to irreversibility. This phenomenon emerges from three different sources:

- Ohmic losses occur due to the electrical resistance of the electrodes and electrolyte and the ionic resistance of the electrolyte. This resistance leads to a voltage drop that reduces the cell's voltage output.
- Activation losses are related to the activation energy required for the electrochemical reactions at the electrodes to proceed. This energy barrier must be overcome for the reactions to take place and results in a voltage loss.
- Concentration losses result from the limited transport of reactants to the electrode surfaces or products away from them, leading to a concentration gradient and, consequently, a voltage drop.

Different metrics are used to analyze polarization losses, quantifying resistive, kinetic and output specificities of SOCs. The most relevant metrics are Rs, Rp, ASR and power density:

- Rs (Series Resistance): Indicates the ohmic resistance of electrolyte, electrodes, and interconnects. It is originated from ionic transport in the electrolyte and provokes voltage drop with current, and because of this it's necessary minimize Rs in order to reduce ohmic losses.

- Rp (Polarization Resistance): Represents resistivity related to electrode reaction kinetics. It originates voltage losses due to activation barriers and gas diffusion limitations and because of this is essential to lower Rp in order to accelerate electrode reaction and reduce polarization losses.

- ASR (Area-Specific Resistance): Consists in the sum of Rs and Rp (total resistance) normalized to the electrode area, providing a comparison between different cell sizes and designs ($\Omega \cdot cm^2$). The aim is to reduce ASR values in order to improve electrochemical efficiency.

- Power Density: Defined as the power generated per unit area (W/cm^2). Demonstrates overall cell efficiency and calculated as the product of current density and voltage. For practical SOC studies it's a priority to maximize power density [9–14].

1.2.3 Chromium effects on cell performance

Although electrode materials containing chromium are widely studied, they showed to cause significant issues, as Cr can volatilize at higher temperatures and create a solid deposit on the electrode, reducing the cell's stability and performance degradation. Due to this fact, an emergent interest for Cr free compositions started to take place, as mitigating poison effects and enhancing cell durability was important for the advance of future research. The present work investigates both electrode materials with and without chromium compositions, with the objective of evaluating its effect on the cell's electrochemical performance and stability, using hydrogen as a fuel under SOC conditions. [3, 9, 10, 15–17].

1.3 SOFC Composition (Materials)

A cell is made out of two electrodes (oxygen electrode and fuel electrode) and an electrolyte in between and has the purpose of producing electricity by supplementing it with a fuel (SOFC) and can also be used for the opposite reaction, providing the cell with an electric current and producing the desired products (SOEC). SOCs can be implemented in several different devices such as portable power generators, automobiles, or power plants and typically operate at 80–95% to reach maximum efficiency. The design of the cell, as well as the morphological characteristics of the electrodes and electrolytes, are fundamental to the efficiency and proper functioning of the cell. Cell components in general must exhibit low resistivity (lower than 0.5 ohm·cm), low cost, thermal compatibility, and high durability. HEOs are a promising technology attributed to their ability to have multiple cations into a single phase structure, delivering desired properties such as chemical and thermal stability. These materials demonstrate a high affinity for SOCs due to the fact that under both oxidizing and reducing conditions, the crystal structure can be stabilized by their configurational entropy while maintaining adequate electronic and ionic conductivity

under a vast range of oxygen partial pressures. SOCs can also be highly doped, allowing incorporation of a wide range of elements from the periodic table, with perovskite-type structures being among the most widely used. These structures must provide stability in both oxidizing and reducing atmospheres, as well as sufficient electrical conductivity across a wide range of O_2 partial pressures [3, 9–11, 13, 14, 18].

1.3.1 Oxygen Electrodes

The Oxygen Electrodes (OEs) are the place where the oxygen reduction or evolution reaction occurs, depending on the mode of operation. There are several properties that are sought when choosing an OE for SOCs, namely mixed ionic-electronic conductivity (MIEC) to provide faster charge transport, high catalytic activity for Oxygen Reduction Reaction (ORR) and Oxygen Evolution Reaction (OER), low resistance for each step of these reactions (total resistance $< 0.5\,\Omega \cdot \mathrm{cm}^2$), high conductivity ($> 100$ S/cm), and sufficient electronic conductivity (> 100, S/cm) to ensure efficient current requirements. OE must also be compatible with the electrolyte/interconnect chemically, thermomechanically and structurally stable over a long period operation. It is also important for the OE to allow efficient gas diffusion and reduce degradation mechanisms such as sulfur poisoning. Some examples of commonly used OEs include the following:

- **Perovskite-type oxygen electrodes** are materials that follow the general formula ABO_3, where A represents the larger atom and B the smaller one. Doping lower oxidation state ions into A and B creates oxygen vacancies, which improves cell performance. Lanthanum strontium manganite (LSM) has been widely studied due to its high stability and catalytic activity at higher temperatures. Lanthanum strontium cobalt ferrite (LSCF) has also gained attention due to its Mixed ionic and electronic conductivity (MIEC), catalytic activity, and high electrical conductivity.

- **Layered perovskite-type oxygen electrodes** are materials with a chemical formula of $AA'B_2O_{5+\delta}$, where A is either a lanthanide or yttrium, A' is Ba or Sr, and B can be Co, FE, or Mn. On one hand, $GdBaCo_2O_{5+\delta}$ (GBCO) has excellent properties such as high electrical conductivity (100–1000 S/cm), ionic conductivity (0.01 S/cm), and catalytic activity of $0.1\,\Omega \cdot \mathrm{cm}^2$ at 700 °C. On the other hand, it is highly reactive with Yttrium-Stabilized Zirconia (YSZ) electrolytes and forms secondary phases with other common electrolytes, affecting cell performance.

- **Double-perovskite-type oxygen electrodes** have either the chemical formula $A_2BB'O_{6-\delta}$ or $AA'BB'O_{6-\delta}$, where A and A' are alkali, alkaline earth, or rare earth ions, and B and B' are metal ions. These OEs have interesting properties for SOC applications, such as high electronic conductivity due to increased oxygen vacancies and stabilization of multivalent ions. $Ba_2CoMo_{0.5}Nb_{0.5}O_{6-\delta}$ (BCMN) is a promising example because it possesses high catalytic activity, although with very low conductivity [3, 9, 10, 19–24].

1.3.2 Fuel Electrodes

Fuel Electrodes (FEs) must have specific characteristics such as high porosity for the transfer of reactants from the electrolyte and products from the reaction area, high electrical conductivity (higher than 10 $S \cdot cm^{-1}$) to enable electron flow between electrodes, as well as good electrocatalytic properties to facilitate the reaction. They should also be chemically and structurally stable to prevent electrode degradation, as well as compatible with the electrolyte and interconnect in terms of thermal expansion at high temperatures. A few examples of commonly used FEs include:

- **Ni-cermet Fuel Electrodes** are commonly used in the form of Nickel oxide-yttria-stabilized zirconia (NiO-YSZ) due to their suitable properties, such as sufficient porosity and uniform distribution of pores, which enable ion transfer and reduce energy losses, high electronic conductivity, catalytic activity, and good stability.
- **Perovskite-type Fuel Electrodes** exhibit low catalytic activity, low conductivity, and instability in certain environments. $La_{0.5}Sr_{1.5}MnO_{4+\delta}$ (L5S15M) and $La_{0.5}Sr_{0.5}Fe_{0.8}Ni_{0.1}Nb_{0.1}O_{3-\delta}$ (LSCFNN) have shown potential in some experiments but lacked reliability in terms of catalytic activity. Another example is $Sr_2CrMoO_{6-\delta}$, which showed higher conductivity but much higher resistance for these reactions.
- **Cu-cermet Fuel Electrodes** are usually used when hydrocarbons are used as fuel. $Cu–CeO_2–TSZ$ provides three times the efficiency of Ni-cermet FEs, although when using H_2 as fuel, it exhibits similar catalytic activity, demonstrating great reliability [3, 9, 17, 19, 23, 25, 26].

1.3.3 Electrolyte

The electrolyte is crucial to the functioning of a cell because it serves as a pathway for ions to flow between electrodes due to the potential difference, enabling the electrochemical reactions while also preventing direct mixing between the fuel and oxidant. Different electrolytes are typically selected based on certain properties, such as high ionic conductivity, chemical and thermal stability, compatibility with electrode materials, and low electronic conductivity to prevent current leakage. There are different types of electrolytes, and among the most studied ones are oxide-ion conductors, such as fluorite, perovskite, and apatite structures [9, 19, 27].

1.3.4 Interconnectors

Interconnection plates are used for conduction of electrons between the different components of the cell and so they need to have specific characteristics that can provide those connections in a consistent way, such as high electrical conductivity, chemical stability for both oxidation and reduction atmospheres, similar thermal expansion coefficient as the other cell components, low cost and high effectiveness. In addition, interconnector plates

are mainly used to electrically connect multiple single cells into stacks, enabling higher power output at the system level. Lanthanum chromite ($LaCrO_3$) is commonly used as an interconnection material as it possesses the desired properties previously referred [3, 28–30].

1.3.5 Barrier Layer

Barrier Layers (BLs) are thin protective layers placed at the electrolyte-electrode interface to prevent cation interdiffusion. During cell manufacturing at high temperatures (1000–1500ºC), electrode elements can react with the electrolyte, leading to degradation and reduced performance. A commonly used BL is Ceria-Gadolinia (CGO), which can be deposited using traditional methods like screen-printing and tape casting (resulting in less dense layers) or advanced techniques such as magnetron sputtering and Pulsed Laser Deposition (PLD) for more effective and denser layers. CGO improves component compatibility, enhances durability, and increases power density [19, 27, 31–33].

1.3.6 Sealants

Sealants are used to keep the gas contained in the inner part of the cell and not let it leak to the outside. These leakages are related to fractures due to extreme thermal conditions, thermal expansion, or thermal treatments. Because of this, it's important to have sealants with certain properties in order to be reliable in every situation. High-quality sealants must be stable and chemically compatible with other cell components and have low thermal expansion [3, 27].

1.4 SOFC Cell Architecture

SOCs can have different designs and configurations. Design-wise, they are categorized into two main aspects: stack configuration and cell support. Functionally, they can be classified based on three main criteria: flow of reactants, temperature range, and charge carrier type. These cells also follow standard configurations such as planar, tubular, or monolithic designs [3, 9, 10].

1.4.1 Standard designs

- **Planar design** is a flat structure with two layers of electrodes with one layer of electrolyte in between, where the fuel is supplied in the center or from the edges, depending on whether the cell is circular or squared, respectively. This design has some advantages such as being easy to manufacture, low cost, low ohmic resistance, and enabling high power. However, the sealing process is more complicated, so the risk of leakage is higher, and thermal resistance is much lower.

- **Tubular design** is a tubular structure composed of an inner and outer layer of electrodes and a middle one made out of electrolyte. Fuel is supplied on the outer layer while an air atmosphere is injected on the inner layer. This design has better structural resistance and doesn't need a sealant, but also enables lower power and higher ohmic resistance.

- **Monolithic design** is the most complex design, where the fuel and air flow in different directions in a shape similar to a heat exchanger. This design has many downsides, as it is costly and has low ionic conductivity [3, 27, 31, 34, 35].

1.4.2 Cell structure support

In terms of cell structure, SOCs can be categorized based on whether they are self- or externally supported. The self-supported ones have a thick layer providing support for the cell. The thick layer can be a present in the electrode (electrolyte-supported), in the anode (anode-supported) or cathode (cathode-supported):

- **Electrolyte-supported cells** have a thick electrolyte layer which provides the cell with better endurance but less conductivity due to higher ohmic resistance and because of that requires higher temperatures to operate.

- **Anode-supported cells** have a thin electrolyte layer, providing better conductivity, lower ohmic losses, stability, and heat flow but increased degradation over time and a smaller lifespan compared to cathode-supported cells.

- **Cathode-supported cells** have a similar configuration as anode-supported cells have longer longevity but often require higher fabrication costs and lower efficiency.

External supported cells have an additional layer made of metal or substrate to provide the needed support. This additional layer uses thinner electrochemical layers and even though it allows lower operating temperatures, it's still vulnerable to corrosion [3, 27, 34–36].

1.5 Symmetrical Cells

Symmetrical SOCs differ from other state of the art anode supported cells by having the same kind of electrode material (symmetrical) at both the OE and FE. This technology has shown growing potential to enhance thermochemical compatibility of electrodes and electrolytes, reduce degradation due to coking and sulfur poisoning, and lower fabrication costs. By employing the use of single electrode material also simplifies cell design, although some challenges can appear due to the fact that electrode materials must keep a good stability under both oxidizing and reducing conditions.

However, there are several cathodes that demonstrate good performance under ORR conditions but are unreliable under reducing atmospheres. Because of this, most symmetrical SOFCs are made of anodic oxide materials. Electron conduction in these cells is enhanced by doping a metal cation into the B-site of the structure, impacting directly the hopping mechanism carried by the electron, where it travels between B-site cations and O_2 ions. Phase stability is achieved by providing the B-site with high chemical stability in order to resist reduction to its metallic form. Materials that potentially can provide these properties have been studied, for example $LnMO_3$, $SrTiO_3$, $SrFeO_{3-\delta}$, or $SrCoO_{3-\delta}$ based oxides.

Regardless, HEOs have shown the ability to incorporate multiple cations and stabilize single phase structures, which could be a promising alternative since in order to combine sufficient stability for symmetrical operation, within the existing technology only a limited number of oxygen electrode materials have demonstrated these desired characteristics [10, 37–40].

1.6 High-Entropy Oxides (HEOs) for Oxygen Electrodes

HEOs are a new variety of materials that are gaining the attention of the scientific community due to their potential to enhance the state-of-the-art technologies in this sector. A high entropy configuration is obtained by doping in its structure five or more elements with similar molar fractions. The stability of this complex configuration is obtained from entropy stabilization, where the formation of a single phase solution is preferred over phase separation due to the entropy influence (ΔS_{mix}) lowering Gibbs free energy (ΔG_{mix}). Different crystal structures can be present in HEOs depending on the cation selection, such as perovskite, fluorite, and spinel. Specifically, the perovskite type structure for oxygen electrodes are one of the most promising due to the fact that they gather favorable conditions for cell performance such as flexible catalytic activity and ORR/OER reactions for the oxygen reduction, mixed ionic-electronic conductivity and high stability in both oxidizing and reducing atmospheres.

This combination of different elements also has its downsides, causing structural distortion affecting some properties such as conductivity, catalytic activity, or diffusion. State-of-the-art technologies face some issues related to degradation by reaction to the interlayers or deactivation by pollutants, and HEOs show high potential to overcome those problems.

Various studies have confirmed some of these promises. A report coming from Shao et al. (2022) demonstrates perovskite HEOs with improved catalytic activity and stability under SOFC conditions, while another report coming from Tarancón et al. (2024) illustrated an enhanced redox tolerance of HEO oxygen electrodes in symmetrical SOCs configurations. These studies demonstrate that in both SOFC and SOEC applications, perovskites stabilized by the effect of entropy can offer a promising solution for more durable and efficient oxygen electrodes [27, 37, 41, 42].

1.6.1 Fundamental ideas of High Entropy Oxides

In order to reach a certain stability of a solid mixture, it is important to minimize the Gibbs free energy (ΔG_{mix}). This energy parameter is strictly related to the enthalpy (ΔH_{mix}) and entropy (ΔS_{mix}) of the mixture, as well as the absolute temperature (T):

A general criteria to determine if a material is a HEO is if $\Delta S_{mix} \geq 1.5R$. It's very common in systems where five or more different elements are present. With a similar molar proportion between the different elements, the entropy can be significantly increased and maximized [37, 42–44].

1.6.2 High entropy ceramics structures

Solid oxide cell structures for high entropy oxides can have different configurations and elements that give stability to the cell through entropy. There are various examples of these structures, such as fluorite, perovskite, or spinel. Other structures like rock-salt or layered O_3 type have shown high potential to improve the commonly used technology, as illustrated in Figure 1.1:

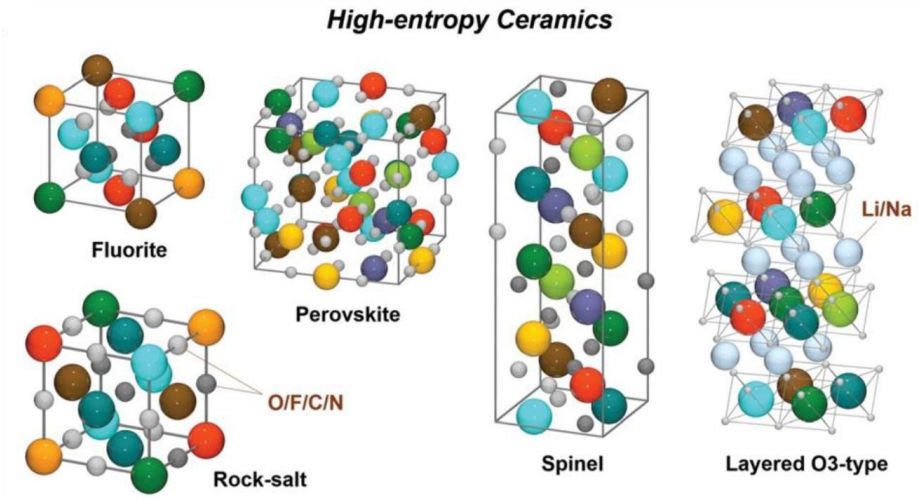

Figure 1.1: Examples of high entropy ceramics structures [27]

- **Fluorite HEOs** are composed of between three and seven cationic elements with the general formula MX_2, where M is a metal cation and X is an anion. Examples include stabilized zirconia doped with yttrium (T^{3+}) or cerium (Ce^{4+}). These materials have been widely studied as electrolyte materials in SOFCs due to their high ionic conductivity and excellent chemical stability.

- **Perovskite HEOs** have the general formula ABO_3, where A is usually a larger alkaline earth or rare earth cation, and B is a transition metal cation. High entropy perovskites are promising as electrode materials due to their good mixed ionic and electronic conductivity as well as catalytic activity.

- **Spinel HEOs** with general formula AB_2O_4, where A and B are cations of different valences, have shown enhanced thermal stability and catalytic properties, making them promising candidates for SOC applications [37, 42, 43, 46].

1.7 Scope of the thesis

This project aims to test solid oxide cells using two different high-entropy oxide electrodes in both SOEC and SOFC modes. One of the electrode powders, HEO-5 contains chromium, (Gd, Sr, Nd, Sm)(Co, Cr, Fe, Mn, Ni) O_3 while HEO-7 does not, (Gd, Sr, Nd, Sm)(Co, Fe, Mn, Ni)O_3. HEO-5 was set up in a symmetrical cell, whereas HEO-7 was assembled in an anode-supported cell. Afterwards, if the HEO-7 anode-supported cell showed good performance, further testing would be done in a symmetrical configuration. The electrode powders underwent morphological and structural experiments, while the respective cells were subjected to electrochemical tests in both SOFC and SOEC modes. The results were analyzed and compared with similar cell findings in an attempt to improve existing technology.

2

Materials and methods

2.1 Cell Preparation

To create a cell with the desired characteristics, the process begins with electrode paste and Ceria-Gadolinia (CGO) spray preparation, followed by electrode and cell assembly, and concludes with furnace treatment.

- **Cell functionalization**: The paste formulation is similar for both electrode powders and consists of 50% powder and 50% solvent, where 50% of the solvent is terpineol and the other 50% is ink vehicle from fuel cell materials. 200 g of electrode powder, 100 g of ink vehicle from fuel cell materials, and 100 g of terpineol were used. The powder was added to the solvents inside a beaker and mixed using a magnetic stirrer at around 500 rpm overnight.

  For the High Entropy Oxide 5 (HEO-5) Solid Oxide Fuel Cell (SOFC) mode, the same powder previously used for Solid Oxide Eletrolyzer Cell (SOEC) mode was subjected to ball milling to reduce the number of agglomerates. This involved mixing the powder with ceramic spheres, sand, and ethanol in a ball mill machine (*Retsch MM400*), as illustrated in Fig 2.1 (a). After milling, the powder-ethanol mixture was recovered and allowed to dry, yielding the milled powder for cell implementation.

- **Spray preparation**: The spray coating solution was composed of 0.200 g of CGO (barrier layer), 4 g of ethanol, and 0,004 g of PVP. This mixture was stirred with a magnetic stirrer and then placed in an ultrasound bath (*Elmasonic X-tra 30H*) at 25ºC for 15 minutes, as seen in Fig 2.1 (b).

- **Electrode and cell assembly**: Firstly, rounded cells made out of 1g of compressed powder from each High Entropy Oxide (HEO) were used in this experiment. A sheet of parafilm was cut with a punching machine to a diameter of 14 mm and used around the cell base. For the HEO-5 electrode cell, a CGO barrier layer sheet was placed on the cell, and three layers of the electrode solution were applied until a total of 0,020 g of powder was deposited (corresponding to a 20-40 μm electrode layer). Application was done on a 50ºC hot plate to accelerate drying, as demonstrated in Fig 2.1 (c). Each layer was allowed to dry before the next was applied, with the cell

weighed after each step to ensure the weight change reflected only the electrode powder and not residual moisture. The same procedure was applied on both sides of the cell. For the High Entropy Oxide 7 (HEO-7) electrode cell, a single electrode solution layer was applied using a 3D printer (*makeshift automated airbrush with Print 3D Print Solutions*), followed by a sprayed CGO solution layer to create surface roughness.

- **Electrode heat treatment**: After assembling both cells, they were placed in a high-temperature furnace (*Lenton Thermal Designs*) with the purpose of sintering the electrodes, as seen in Fig 2.1 (d). The temperature was increased at a rate of 3ºC/min from 20ºC to 500ºC over 30 minutes, then continued rising at the same rate from 500ºC to 1150ºC over 2 hours. Finally, the cells were cooled down at a rate of -3ºC/min from 1150ºC to 50ºC.

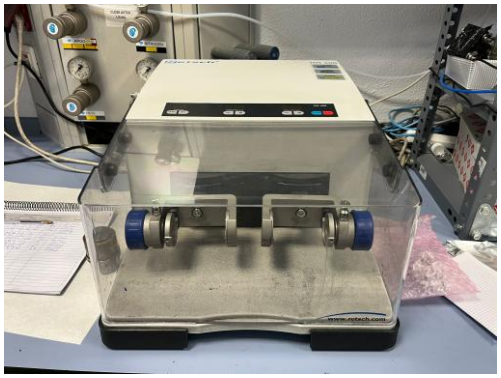

(a) Ball milling

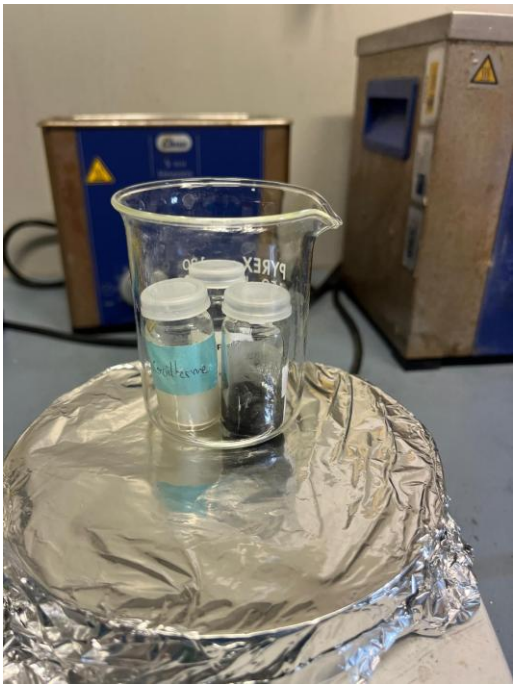

(b) Ink preparation

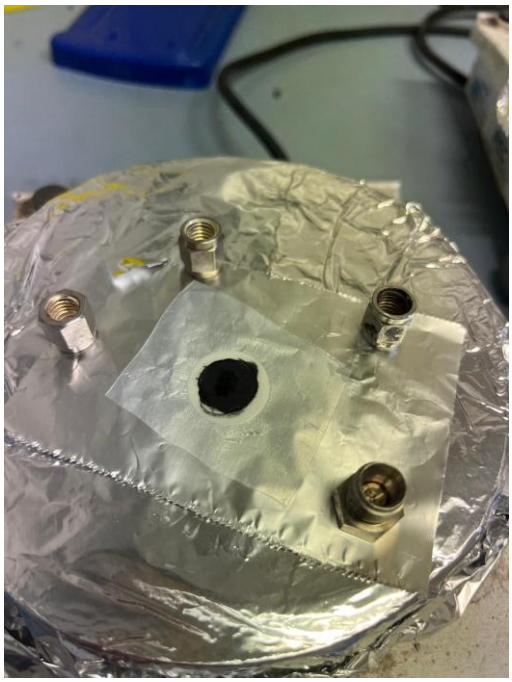

(c) Cell functionalization

(d) Thermal treatment

Figure 2.1: Steps in electrode processing and cell preparation.

2.2 Structural and Morphological Experiments

2.2.1 X-ray diffraction

X-ray diffraction is a technique used to analyze the crystalline structure of HEOs with a device designed for this purpose, also illustrates in Fig 2.2: *Bruker D8 Advanced Diffractometer (USA)* with Cu Kα radiation (λ = 1.5418 Å). An X-ray beam hits the sample's atoms, causing radiation to scatter at different angles and intensities. The information obtained from the diffracted beam is crucial to determine phase composition, structure, and other material characteristics.

To prepare the sample, a spatula was used to introduce some powder into an Eppendorf tube, which was then half-filled with isopropanol. The mixture was stirred and placed in an ultrasound bath for 10 minutes. The resulting solution was deposited onto a silicon support, allowing the liquid to evaporate. Finally, the sample was analyzed in the X-ray diffraction (XRD) machine, with the laser scanning angles from 20º to 90º.

Figure 2.2: X-ray diffraction machine

2.2.2 Scanning Electron Microscopy (SEM)

Scanning Electron Microscopy (SEM) is a technique that provides material analysis at a morphological and compositional level. During this study, two different SEM modes were used: Secondary Electron Detector (SED) for surface morphology and texture, and Energy Dispersive X-ray (EDX) analysis for elemental composition.

Energy dispersive X-ray analysis is performed in the *ZEISS Auriga 60 Field Emission Scanning Electron Microscope* equipped with an energy dispersive X-ray spectrometer (*Oxford X-Max, UK*), as shown in Fig 2.3. This method analyzes the elemental composition of materials by emitting a high-energy electron beam onto the sample, which excites the atoms and causes them to emit characteristic X-ray spectra. The detector captures

these spectra, enabling identification and quantification of the elements present. This method confirms elemental presence, composition ratios, segregations, and possible contamination in the powder.

Secondary electron detection in the Scanning electron microscope (SEM) involves hitting the sample surface with an electron beam, causing the emission of low-energy secondary electrons, which are detected and converted into a signal. The resulting image reflects surface topography and material properties such as texture and roughness.

A sample of the remnants of the HEO-5 symmetrical cell after degradation was taped onto an observation support and examined inside the SEM under high vacuum. High-resolution images were taken of the entire cell layers and the structural phases of each electrode.

Figure 2.3: Scanning Electron Microscope (SEM)

2.3 Electrochemical Characterization

For the following experiments, the cell was placed in a setup simulating SOFC/SOEC modes on a smaller scale on a device called ProboStat, as shown in Fig 2.4 (b). This setup allows different atmospheric conditions on each side of the cell without gas exchange between the inner and outer chambers. Electrical connections were made using gold meshes attached with wires on both sides of the cell to introduce and retrieve current. A thermocouple was placed next to the cell to monitor temperature.

For the HEO-5 electrode, the cell surfaces were coated with a mixture of gold and isopropanol to facilitate electrical contact. The cell was then placed over the inner chamber with the gold mesh on top and left to dry (gold was chosen for its inertness with the electrodes).

The cell was glued into the ProboStat to seal the inner chamber from the outer chamber, where two different atmospheres were maintained. A weight pressed the cell during glue drying (two layers were applied). The thermocouple was connected and placed near the cell, and the other gold mesh was placed on top to complete the circuit.

Connection integrity was checked with a multimeter. A triangular structure with an attached tube supplied the secondary gas atmosphere. A cylindrical cover created the outer chamber. The complete setup was placed in a furnace (*Lenton Thermal Designs*) with an added heat retention cover, as demonstrated in Fig 2.4 (a).

To ensure the proper sealing, the temperature was ramped gradually according to the sealant specifications: first to 93ºC at 1ºC/min, then dwelled 2 hours; then to 260ºC, dwelled 2 hours; finally to 900ºC and held steady. ProboStat cables were connected to a potentiostat/galvanostat for Electrochemical Impedance Spectroscopy (EIS) and polarization curve measurements. Thermal bands were wrapped around tubes carrying water vapor to prevent condensation.

In SOEC mode, one side of the cell received 40 mLn/min of air mixed with 40 NmL/min of argon (inert carrier), and the other side was supplied with increasing water vapor flow, rising by 500 NmL/min every 5 minutes until 40 NmL/min was reached.

For the HEO-7 anode-supported cell, both SOFC and SOEC modes were tested. For SOFC, NiO was first reduced to Ni using a mixture of air and hydrogen (air flow at 200 NmL/min was 2.5 times that of hydrogen at 80 NmL/min) with water vapor supplied to the opposite electrode. To switch to SOEC, the polarity was inverted to start electrolysis. Flows were 20 NmL/min argon, 12.5 NmL/min hydrogen, 150 NmL/min air, and 5 g/h water vapor.

A similar procedure was followed for the HEO-5 SOFC mode.

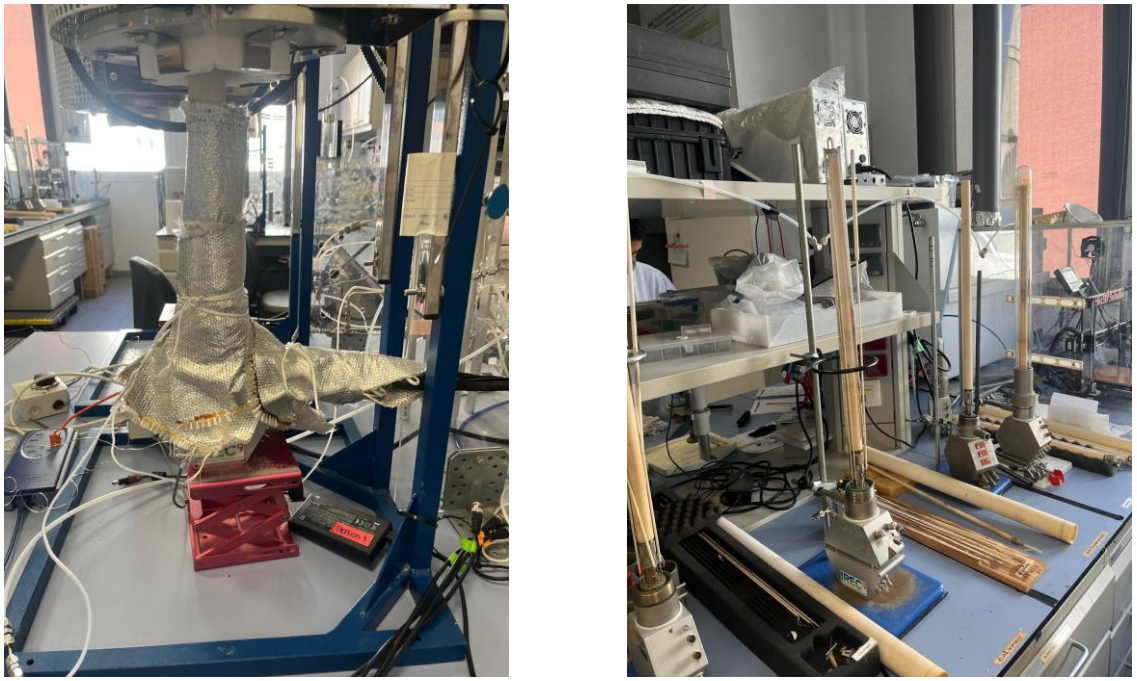

(a) Furnace station (b) ProboStat

Figure 2.4: Electrochemical experiments preparation

2.3.1 Electrochemical impedance spectroscopy

EIS is a technique used to study the electrical properties of HEOs by applying a small AC voltage to the cell and measuring the impedance, which can be separated into real resistance and imaginary capacitance components. This data is essential to determine how ions move through the material and how easily electrons move at the electrode/electrolyte interface, as well as its energy storage potential.

Using an amplitude of 50 mA AC, the frequency range was set from 100 kHz to 0.1 Hz, focusing on electrode performance analysis. The potentiostat recorded data and generated characteristic impedance arcs.

In SOEC mode, using HEO-5 and HEO-7 anode-supported symmetrical cells, the temperature was decreased from 900ºC to 750ºC in 50ºC steps. Measurements were taken at applied voltages of 1.2 V, 1.1 V, and open circuit voltage (OCV) at each temperature. Graphs were plotted from the recorded data.

In SOFC mode with a HEO-7 anode-supported cell, a similar procedure was followed but with applied voltages of 0.7 V, 0.8 V, 0.9 V, and OCV at each temperature.

2.3.2 Polarization Curves (IV Curves)

Polarization curves analyze electrode behavior and efficiency by applying a potential to the cell and measuring the resulting current. The curve can be divided into three regions:

- **Activation region**: Electrochemical reactions at the electrode surface cause rapid current increase with voltage.
- **Ohmic region**: Linear current rise proportional to voltage reflects cell resistance.
- **Mass transfer-controlled region**: Current rise slows due to diffusion limitations of ions to the electrode surface.

This analysis helps determine electrode suitability in oxidizing and reducing environments (reaction kinetics), susceptibility to corrosion, and overall reaction kinetics.

The system was set with a maximum voltage of 1.5 V, a ramp rate of 0.1 A/s, 1 s intervals, current range 0-5 A, and a step size of 0.025 A. Temperature was decreased from 900ºC to 750ºC in 50ºC steps. Current and voltage data were recorded, and current density was calculated by dividing current by electrode surface area.

2.3.3 Cell Degradation

Degradation studies monitor changes in cell performance over time, providing insight into material durability and long-term operation viability.

Measurements were taken by maintaining the cell at 900ºC and 0.7 V for SOFC mode or 1.2 V for SOEC mode. Current density and voltage were recorded every 10 minutes over a 24 hour period. Degradation rates were evaluated by analyzing the decrease in current density and changes in voltage over time.

3

Discussion of Results

In this section, morphological and structural results from the XRD, Energy Dispersive X-ray (EDX), and SED (SEM) for HEO-5, and XRD for HEO-7, were analyzed. Electrochemical results were gathered from the EIS and IV curves for HEO-5 and HEO-7 in both symmetrical and anode-supported configurations for SOFC and SOEC modes. Degradation results were only analyzed for HEO-5 experiments because the HEO-7 cell broke down a few hours into the process. This data was then compared to similar previous studies, and the different results were discussed.

Different ways were used to better show and compare the obtained results: XRD analysis revealed the orthorhombic crystalline main phase present in the electrode, EDX gave elemental composition maps and Secondary Electron Detector (SED) provides surface morphology images of the cell after degradation, EIS supplied impedance spectra (Nyquist) and Arrhenius plots were built after extracting Rs/Rp vs T from fitted spectra (after equivalent-circuit fitting we extracted Rs and Rp, computed ASR, and summarized these at each temperature and degradation stage), as a comparative table with different Ohmic Resistance (Rs), Polarization Resistance (Rp), and Area-Specific Resistance (ASR) for each temperature and the variation of these values with degradation. For HEO-5 SOFC, a cell performance comparison was made using different inner and outer chamber atmosphere compositions. IV curves were represented in a voltage/current density graph, and degradation results were exhibited in a voltage/time graph where the repercussions of a continuous current input are visible.

3.1 HEO-5 symmetrical cell

3.1.1 Scanning Electron Microscope

The composition results for the HEO-5 were obtained through a XRD analysis. The sample showed pronounced and well-defined peaks, indicating a multi-phase and highly crystalline structure.

Two main phases were distinguished in this analysis. The main phase corresponded to an orthorhombic crystal structure, prominent in the range of 30º to 70º, aligning with

standard orthorhombic phase patterns on HEOs. The highest peak was observed near 32º to 35º, demonstrating preferential orientation or a higher degree of crystallinity in that direction.

The second phase was attributed to a tetragonal phase that appeared to a lesser extent, as several minor peaks stood out around 20º to 30º and past 70º, which could indicate incomplete homogenization or phase segregation during synthesis or cooling. The occurrence of this phase can affect electrode performance and stability through properties like ionic conductivity based on its distribution and interface affinity with the main phase. This analysis is shown in Fig. 3.1.

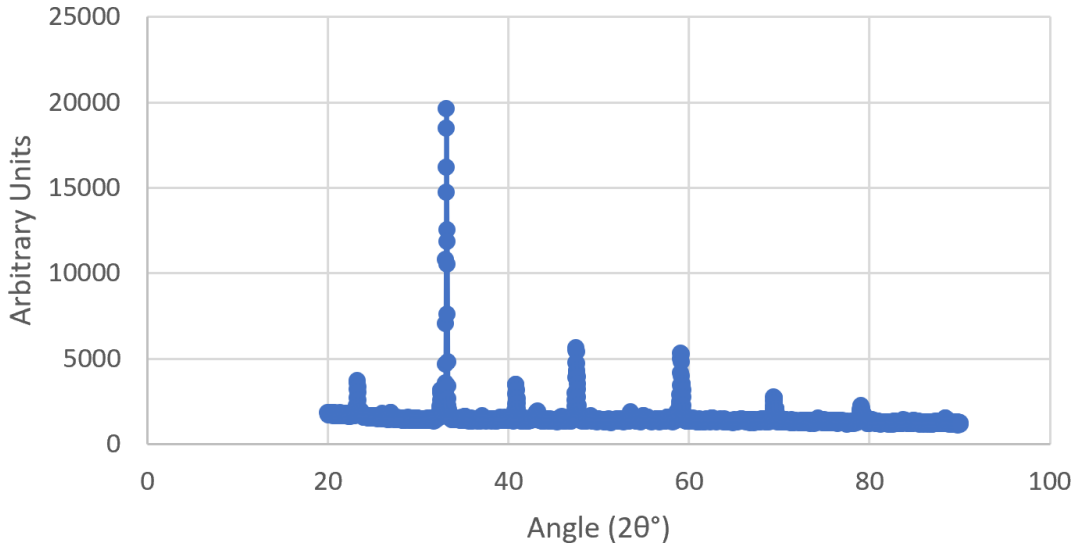

Figure 3.1: X-ray diffractogram for HEO-5

On the other hand, morphology images were obtained using a SED analysis, making it possible to visualize the structural aftermath of the cell after testing and degradation process, by breaking it in a way that it's possible to visualize a cross-sectional part of the interior of the cell. They revealed a rocky and highly porous morphology composed of heterogeneous, poorly developed crystals. These irregularities are a product of a non-ideal synthesis process handled by the electrode provider, which can affect properties like conductivity and stability. A rupture in the electrolyte/electrode interface was observed and might result from deficient electrode settling during preparation or preceding deformation effects, which can significantly affect charge transfer and cell performance.

The electrode's microstructural characteristics emphasize the importance of synthesis optimization to refine particle homogeneity, crystallinity, and interface fixation, aiming to improve stability and overall cell performance. For this reason, the electrode mixture went through a process of ball-milling to reduce the number of agglomerates for further testing in SOFC mode. These images are displayed in Fig.3.2.

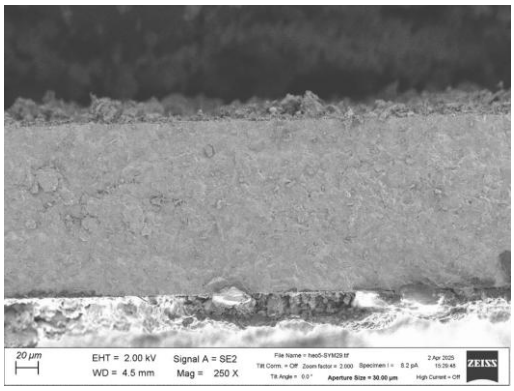

(a) Cross-sectional SEM image showing HEO-5 electrode layers on both the top and bottom surfaces, with the dense electrolyte in between

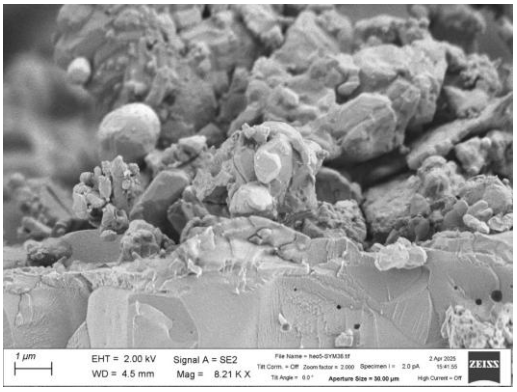

(b) High-magnification SEM image of the top HEO-5 electrode surface

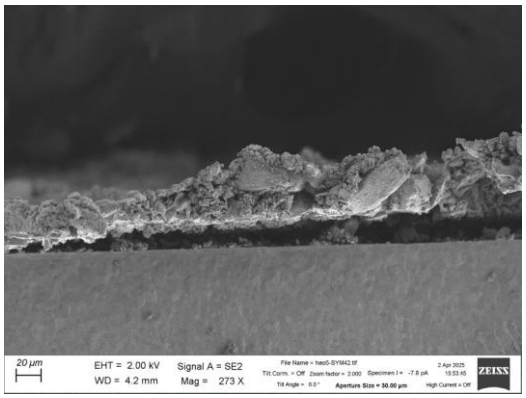

(c) Cross-sectional SEM image showing the top HEO-5 electrode layer above the electrolyte

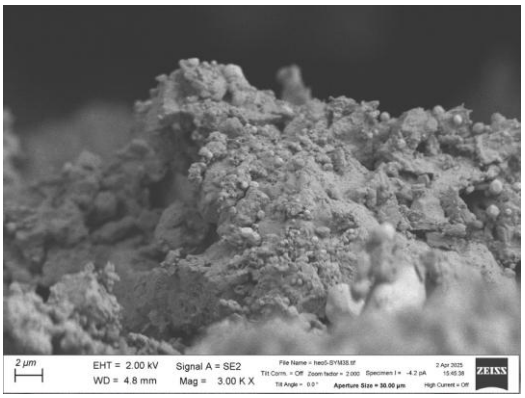

(d) High-magnification SEM image of the top HEO-5 electrode, displaying its porous morphology

Figure 3.2: Secondary Electron Detector (SEM) images of HEO-5

3.2 HEO-5 symmetrical cell in SOEC mode

3.2.1 Polarization Curves

IV curves were recorded at 900ºC, 850ºC, and 800ºC, plotted as current density (A/cm^2) versus voltage (V), both before and after degradation.

As shown in Fig 3.3, pre-degradation results showed improved performance at higher temperatures, with flatter curves and lower ohmic and activation losses. At lower temperatures, voltage increased more rapidly with current density, indicating greater polarization losses. This confirmed that improved ionic conductivity and reaction kinetics enhance efficiency at elevated temperatures.

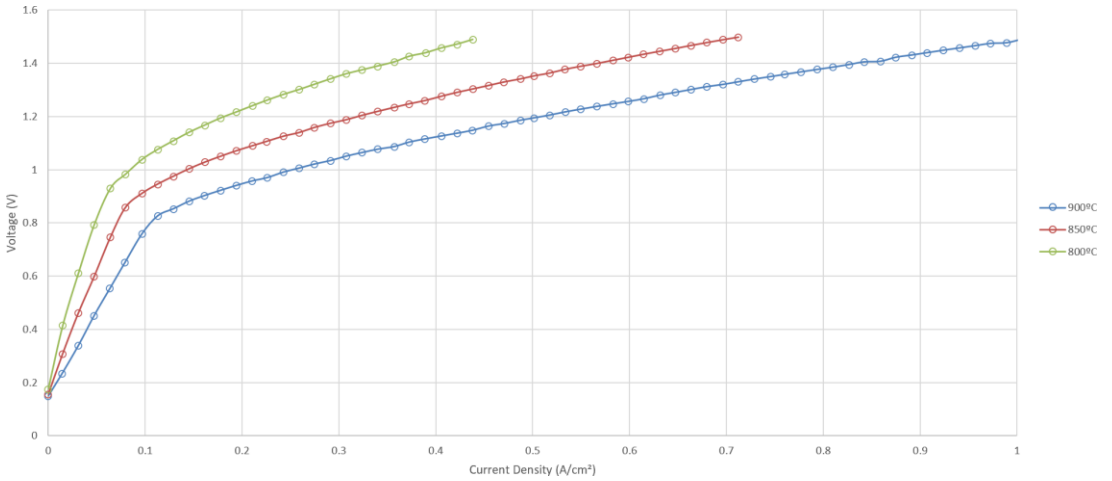

Figure 3.3: Polarization curves at different temperatures for HEO-5 in SOEC mode

3.2.2 Electrochemical Impedance Spectroscopy

The EIS results were analyzed at 1200 mV, considering measurement temperatures of 900ºC, 850ºC, and 800ºC. These measurements were displayed as Nyquist plots, with Real Resistivity (related to electrode resistivity) as Z' (Ω/cm^2), and Imaginary Resistivity (related to inductive behavior and polarization processes) as Z'' (Ω/cm^2), along with their respective fitted curves.

As presented in Fig.3.4, the data were fitted using an equivalent circuit model composed of an inductor in series with four resistors, three of them in parallel with constant phase elements or an inductor in series with three resistors, two of them in parallel with constant phase elements. One model was chosen over the other depending on the number of semicircles exhibited in the Nyquist plot, which corresponded on the number of resistors. This model showed parameter errors below 10% in most cases.

Figure 3.4: Equivalent circuit models for HEO-5 impedance fitting in SOEC mode

The impedance measurements exhibited three depressed arcs corresponding to high, mid, and low frequencies. The high-frequency arc relates to charge transfer resistance at the electrolyte/electrode interface, the mid-frequency arc corresponds to surface exchange or reaction kinetics, and the low-frequency arc is associated with transport processes or gas diffusion. These arcs increased in size with decreasing temperature, indicating improved cell performance at higher temperatures due to enhanced electrochemical activity and reduced polarization losses, as shown in Fig.3.5.

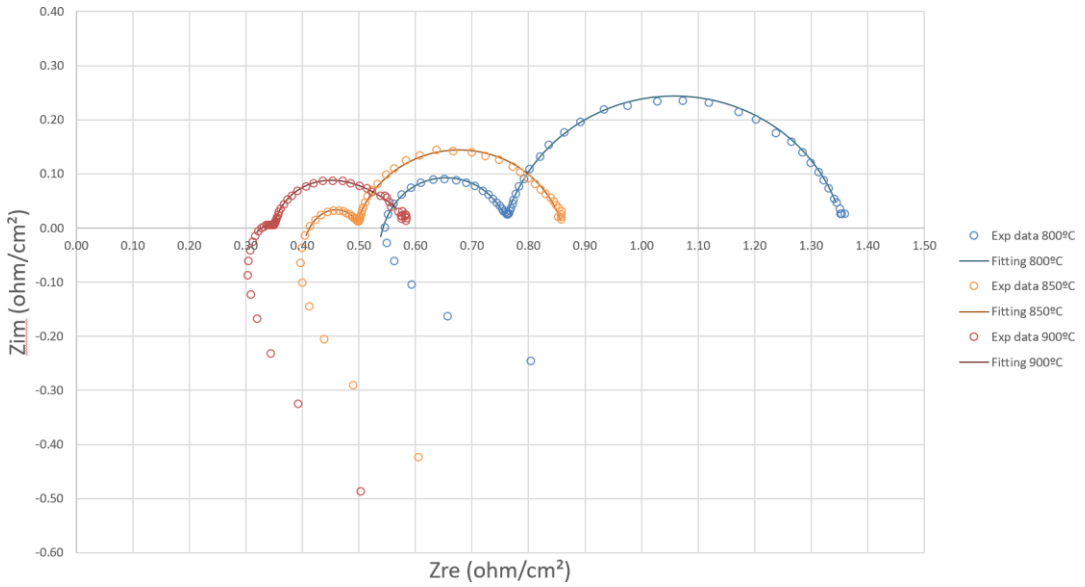

Figure 3.5: Electrochemical Impedance Spectroscopy curves before degradation at different temperatures for HEO-5 in SOEC mode at 1200 mV

3.2.3 Cell Degradation

Degradation was studied after 160 h using a 300 mA current, and from 160 h to 480 h with a 770 mA current at 850ºC. The increased current was chosen because minimal degradation was observed at 300 mA. Data were presented as voltage (V) versus time (h), including a smoothing line to visualize trends.

The degradation process had distinct stages. Initially, up to 160 h at 300 mA, voltage remained steady around 1.0 V, suggesting negligible degradation. Upon increasing the current to 770 mA, voltage gradually rose to about 1.35 V, at an average rate of 0.043 mV/h, revealing clear degradation, mainly due to increased polarization. Nevertheless, the cell exhibited promising stability, with signs of partial recovery rather than irreversible damage. The degradation profile is illustrated in Fig. 3.6.

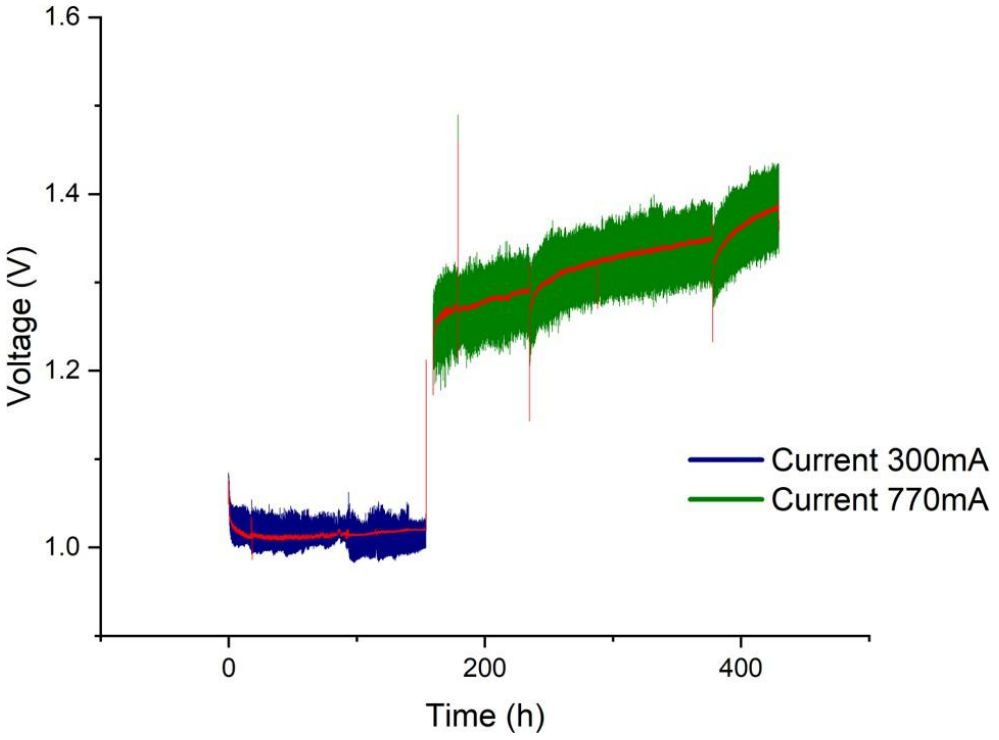

Figure 3.6: Degradation profile for HEO-5 in SOEC mode at 850ºC

To better understand the results for HEO-5, this cell was compared to a similar previously studied symmetrical NMC-GDC|YSZ|NMC-GDC (NMC=$LiNi_{0.33}Mn_{0.33}Co_{0.33}O_2$, *GDC*= $Ce_{0.9}Gd_{0.1}O_{1.95}$) cell was put through a degradation process at 800°C and using a current density of 0.8 A/cm^2 for about 72 h. It had an initial voltage of 1.49 V and came down to 1.42 V at the end, registering the largest voltage loss in the first 10 h. The HEO-5 cell, after the same amount of time, showed a similar degradation loss but at a lower current density: starting at 1.08 V and coming down to 1.02 V at 0.1948 A/cm^2, showing a worse performance overall [19].

3.2.3.1 Cell degradation: EIS/IV

As illustrated in Fig. 3.7, EIS measurements were recorded at multiple degradation points: 0 h, 160 h, 240 h, 350 h, and 480 h. These data were analyzed and fitted to extract values such as Rp and Rs at each stage. A summary table was prepared to better understand the evolution of these parameters over time (Tab.3.1).

Rs corresponds to ohmic losses attributed to the electrolyte, current collectors, and interfacial resistances. It increased from a lower initial value to 0.336 $\Omega \cdot cm^2$ after 480 h. This increase can be linked to degradation in the electrolyte or electrode-electrolyte interfaces due to processes like oxidation, grain boundary resistance, or delamination.

This rise in Rs is visible in the impedance spectra as a rightward shift of the high-frequency arc.

Rp relates to phenomena at the electrode, such as surface reactions, gas diffusion, or charge transfer. It increased from 0.306 $\Omega \cdot cm^2$ initially to 0.324 $\Omega \cdot cm^2$ after 480 h. This rise likely stems from electrode poisoning or elemental diffusion at the interface. The Rp increase is observable through the enlargement of mid- and low-frequency arcs in the impedance spectrum.

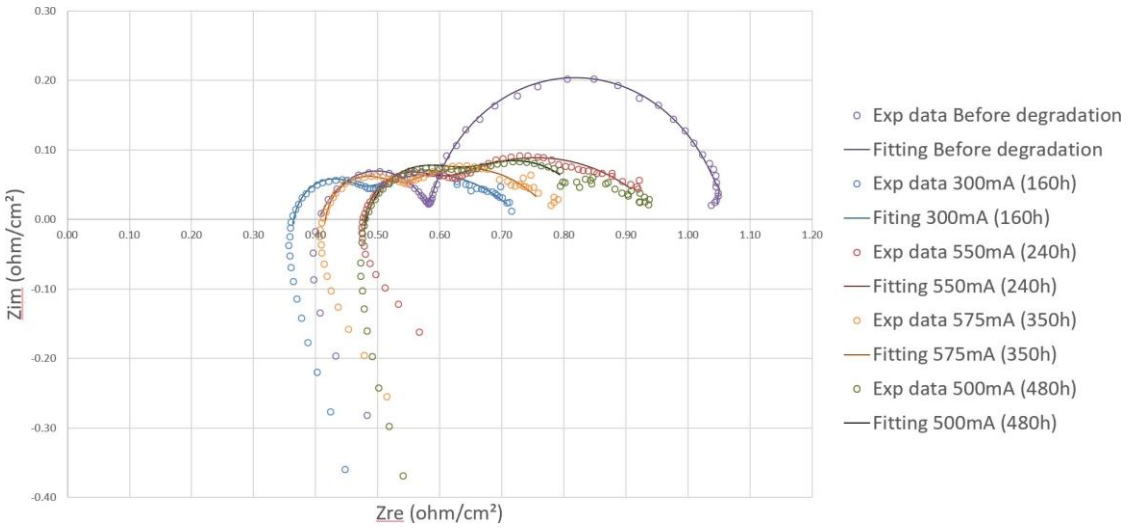

Figure 3.7: Electrochemical Impedance Spectroscopy curves at different stages of degradation for HEO-5 in SOEC mode at 850ºC.

Arrhenius plots were generated to analyze how Rs, Rp, and ASR varied with temperature. The plots displayed three linear trends, where Rp had the steepest slope, indicating that electrode polarization is strongly temperature-dependent. ASR showed an intermediate slope, suggesting that cell resistance improves with temperature, though less dramatically than Rp. Rs exhibited the lowest slope, implying that the electrolyte's ionic conductivity is less affected by temperature, as shown in Fig.3.8. This demonstrates the significance of temperature in optimizing electrode processes.

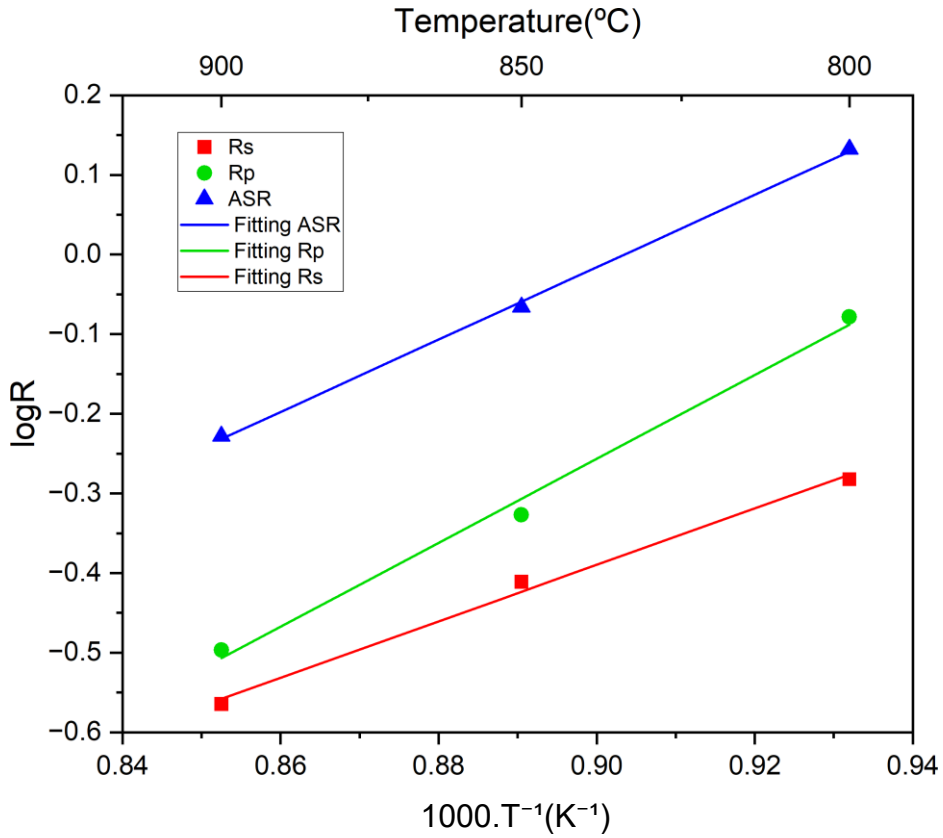

Figure 3.8: Arrhenius plot for HEO-5 SOEC mode

	Temperature (ºC)				Slope	Activation Energy (KJ/mol)
HEO-5 (SOEC)	900	850	800	750		
Rs (Ω)	0.177	0.252	0.339		3.545	29.47313
Rp (Ω)	0.207	0.306	0.542		5.272	43.831408
ASR (Ω·cm²)	0.384	0.558	0.881		4.543	37.770502

Table 3.1: Summary of Rs, Rp, and ASR parameters for HEO-5 in SOEC

To better understand the EIS results for HEO-5, this cell was compared to a previously studied symmetrical cell: LSFN|YSZ|LSFN (LSFN = $La_{0.6}Sr_{0.4}Fe_{0.8}Ni_{0.2}O_3$) using CO_2 as a fuel at 850ºC exhibited an Rp of 0.06 Ω · cm^2 and Activation Energy (Ea) between 0.8 and 1.1 eV. In contrast, the studied HEO-5 cell had an Rp of 0.306 Ω · cm^2 and an Ea of 0.4543 eV. The former showed superior electrode kinetics and lower polarization losses due to the lower Rp, despite the higher Ea, indicating improved performance with increasing temperature [19].

As presented in Fig.3.9, IV measurements taken over time: 160 h, 240 h, 350 h, and 480 h at 850ºC revealed performance decay. Initially, the electrode performed well with low overpotentials. From 160 h onward, higher voltages were required to sustain the same current densities. At 460 h, two experiments were conducted: one started from a stabilized

voltage of 0.13 V and performed better than the other, which began at 0.8 V. At a current density of 0.7 A/cm^2, voltage rose from 1.15 V (initial) to 1.35 V (after 460 h), reflecting increased polarization resistance. Despite the degradation, the electrode maintained high current loads with good stability. Rs and Rp parameters also change over degradation time, as illustrated in Tab.3.2.

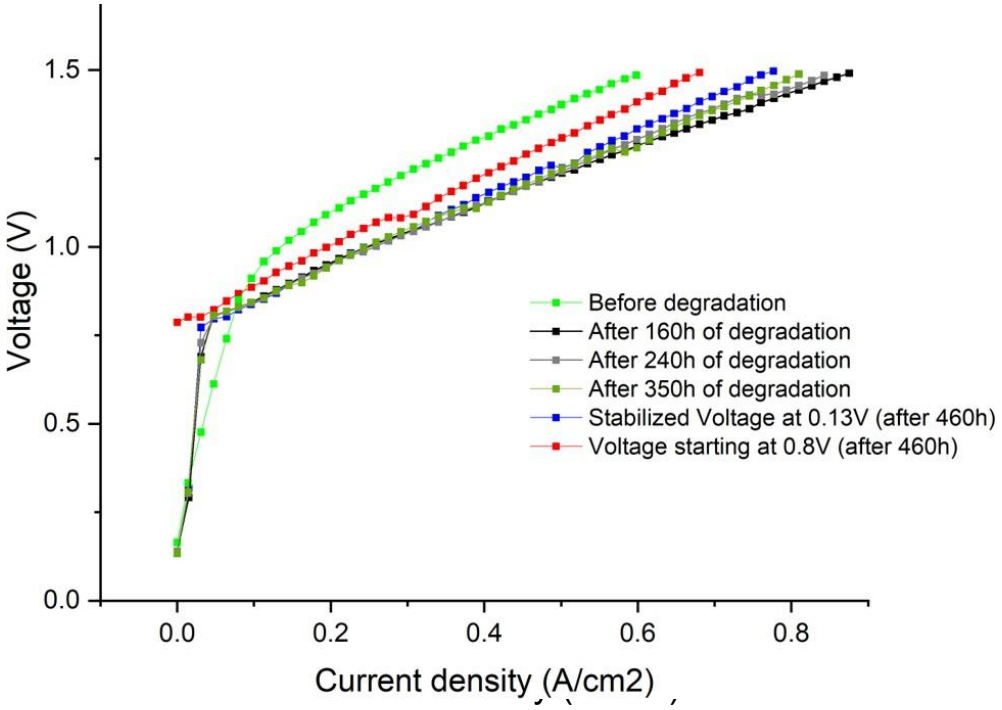

Figure 3.9: Polarization curves at different stages of degradation for HEO-5 in SOEC mode

HEO-5 (SOEC) before/after deg.	0h	480h
Rs (Ω)	0.252	0.336
Rp (Ω)	0.306	0.324

Table 3.2: Summary of Rs and Rp parameters with degradation time

On the other hand, for better understanding IV results, a LSFN|YSZ|LSFN cell previously tested at 850ºC was compared to the studied cell: had a voltage of 1.0 V at a current density of 0.25 A/cm^2, indicating better kinetics and lower losses. In comparison, the HEO-5 cell at the same conditions showed a higher overpotential of 1.16 V [19].

3.3 HEO-5 symmetrical cell in SOFC mode

3.3.1 Polarization Curves

The IV curve results were measured at 900ºC, 850ºC, 800ºC, and 750ºC and displayed as current density (A/cm^2) versus voltage (V), both before and after degradation. Degradation data were collected after 480 h and 780 h at 850ºC, during which a current of 295 mA was applied.

As shown in Fig 3.10, measurements before degradation showed improved performance at higher temperatures, resulting in smoother curves with reduced ohmic and activation losses. At lower temperatures, the voltage dropped more sharply with increasing current density, indicating more significant polarization losses. This suggested that the cell operated more efficiently at higher temperatures due to enhanced ionic conductivity and improved electrochemical kinetics.

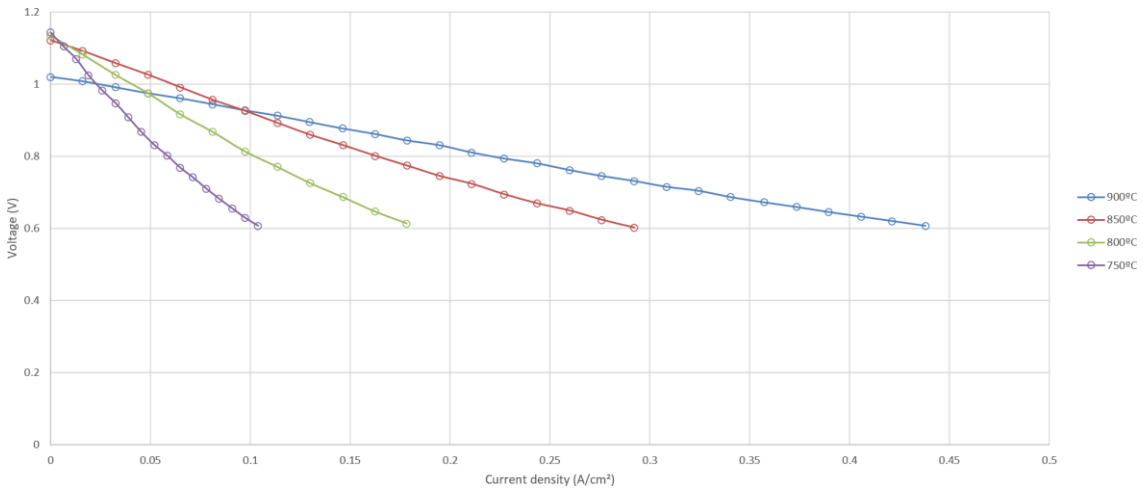

Figure 3.10: Polarization curves at different temperatures for HEO-5 in SOFC mode

To better understand the results for HEO-5, IV curves were also compared to the performance of a previously studied symmetrical LSCM|YSZ|LSCM (LSCM = $La_{0.75}Sr_{0.25}Cr_{0.5}Mn_{0.5}O_3$) fuel cell using wet H_2 at 900ºC. At a current density of 0.25 A/cm^2, the voltage was 0.76 V. The HEO-5 cell demonstrated a similar voltage at the same current density and temperature, indicating comparable electrode kinetics and polarization losses [10].

3.3.2 Electrochemical Impedance Spectroscopy

The EIS results were analyzed at 700 mV and covered measurement temperatures of 900°C, 850°C, 800°C, and 750°C. These measurements were displayed as Nyquist plots, showing Real Resistivity (related to electrode resistivity) as Z' (ohm/cm^2), and Imaginary Resistivity (related to inductance) as Z'' (ohm/cm^2), along with their respective fitted curves: as presented in Fig.3.11, the data were fitted using an equivalent circuit model composed of an inductor in series with three resistors, two of them in parallel with constant

phase elements, or a simpler model composed of three resistors in series with parallel constant phase element. One model was chosen over the other depending on the presence of negative Imaginary Resistivity values exhibited in the Nyquist plot, which corresponded to the presence of an inductor.. These models revealed parameter errors below 10% in most cases.

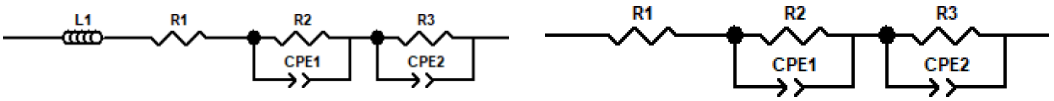

Figure 3.11: Equivalent circuit models for HEO-5 impedance fitting in SOFC mode

The impedance measurements exhibited three depressed arcs corresponding to higher or lower frequencies: the high-frequency arc corresponded to the charge transfer resistance at the interface between the electrolyte and the electrode, the middle-frequency arc corresponded to the reaction kinetics or surface exchange, and the lower-frequency arc to transport processes in the electrode or gas diffusion. These arcs increased in size as temperature decreased, illustrating better cell performance at higher temperatures due to optimized electrochemical activity and lower polarization losses, as shown in Fig.3.12.

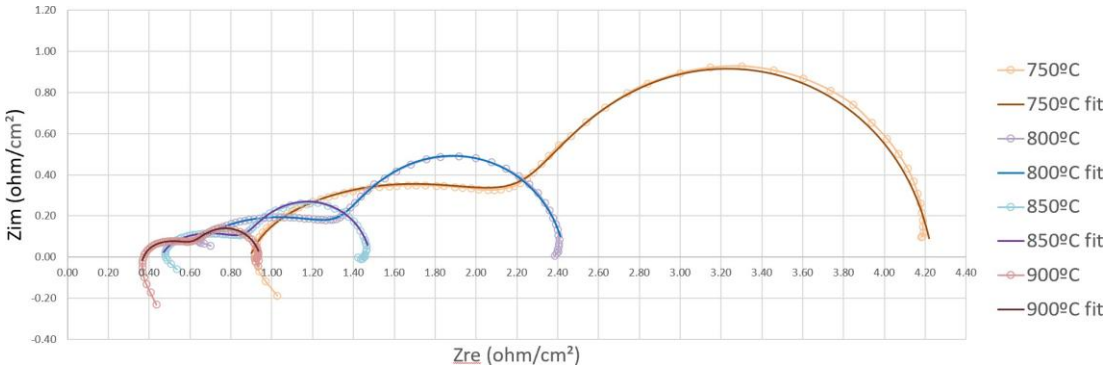

Figure 3.12: Electrochemical Impedance Spectroscopy curves at different temperatures for HEO-5 in SOFC mode at 700 mV

3.3.3 Cell Degradation

Cell degradation data were collected up to 780 h using a current of 295 mA at a constant temperature of 850ºC. The current remained stable throughout. The results were displayed as a voltage (V) versus time (h) plot, with a smoothing line added to illustrate the degradation trend.

The degradation behavior showed distinct decaying trends that gradually stabilized. In the initial phase, up to around 450 h, the voltage gradually decreased from approximately 0.75 V to 0.66 V, suggesting nonlinear degradation. Minor voltage recoveries were observed, possibly due to environmental or operational disturbances. These changes were mainly attributed to an increase in polarization resistance under prolonged current exposure.

At 450h, voltage suffered a significant drop, reaching an approximate value of 0.63 V. From 450h to 780 h, the cell exhibited lower degradation rates and more stable performance, where the voltage ranged between 0.64 V and 0.62 V. Despite the clear degradation in the early phase, the electrode was overall stable, and partial recoveries were more common than irreversible failure mechanisms. The degradation profile is illustrated in Fig. 3.13.

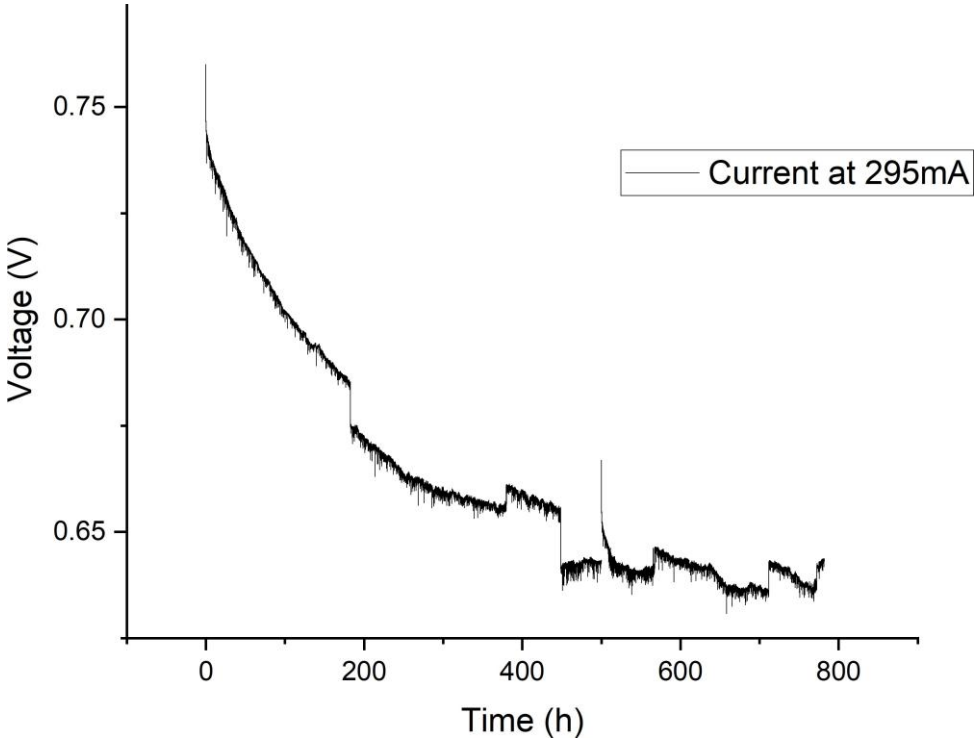

Figure 3.13: Degradation profile for HEO-5 in SOFC mode at 850ºC

To better understand the results for HEO-5, a previously studied symmetrical LSCM|YSZ|LSCM cell was used for comparison. At 800ºC and a current density of 400 mA/cm^2, the voltage dropped from 0.53 V to 0.48 V after 150 h, eventually stabilizing.

In comparison, degradation data from HEO-5 after 125 h showed a smaller voltage drop—from 0.75 V to 0.70 V—at a lower current density of approximately 191.6 mA/cm^2. However, the HEO-5 cell required a longer time to stabilize (230 h), compared to 150 h for the previously studied cell [10].

3.3.3.1 Cell degradation: EIS/IV

As illustrated in Fig. 3.14, EIS measurements were recorded at three different degradation points: 0 h, 500 h, and 780 h. This data was then analyzed and fitted in order to obtain resistances such as polarization resistance (Rp) and series resistance (Rs) at each degradation point. A summary table was prepared to better understand the evolution of these parameters with time (Tab.3.3).

The Rs corresponded to ohmic losses attributed to the electrolyte, current collectors, and interfacial resistances. It showed an increase from 0.268 $\Omega \cdot cm^2$ at the fresh cell state (0 h) to 0.469 $\Omega \cdot cm^2$ after 500 h. This difference can be attributed to degradation in the electrolyte or electrode–electrolyte interfaces due to various inevitable processes such as oxidation, grain boundary resistance, or interfacial delamination. After 780 h, Rs reversed its growth trend and decreased to 0.444 $\Omega \cdot cm^2$, indicating stabilization of the degradation effects on the cell. The overall Rs increase was visible from the impedance spectrum perspective, showing a rightward shift of the high-frequency arc.

The Rp corresponded to phenomena manifesting at the electrode, such as surface reactions, gas diffusion, or charge transfer. It increased from 0.696 $\Omega \cdot cm^2$ before degradation to 1.171 $\Omega \cdot cm^2$ after 500 h, reaching its highest value after 780 h at 1.217 $\Omega \cdot cm^2$. This continuous increase was likely linked to electrode poisoning or element diffusion in the electrode interface. The constant Rp increase over time was also visible through the impedance spectrum, which showed an enlargement of the mid- and low-frequency arcs.

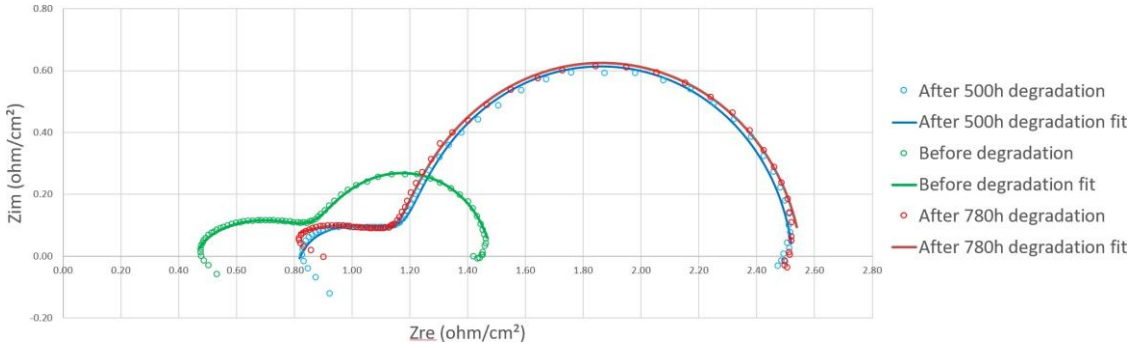

Figure 3.14: Electrochemical Impedance Spectroscopy curves at different degradation stages for HEO-5 in SOFC mode

Arrhenius plots were also included as 1000/T (K^{-1}) versus log(R), to better analyze how Rs, Rp, and ASR parameters evolved under different temperature conditions. The plots displayed three linear fits at the measured temperatures, where Rp had the steepest slope, indicating that temperature highly influences electrode polarization. ASR had an intermediate slope, showing that cell resistance decreases at higher temperatures, but less sharply than Rp. In contrast, Rs had the lowest slope, indicating that the electrolyte's ionic conductivity is less affected by temperature, as shown in Fig.3.15. This suggests that temperature strongly impacts resistance related to electrode processes, highlighting the importance of optimizing electrode kinetics.

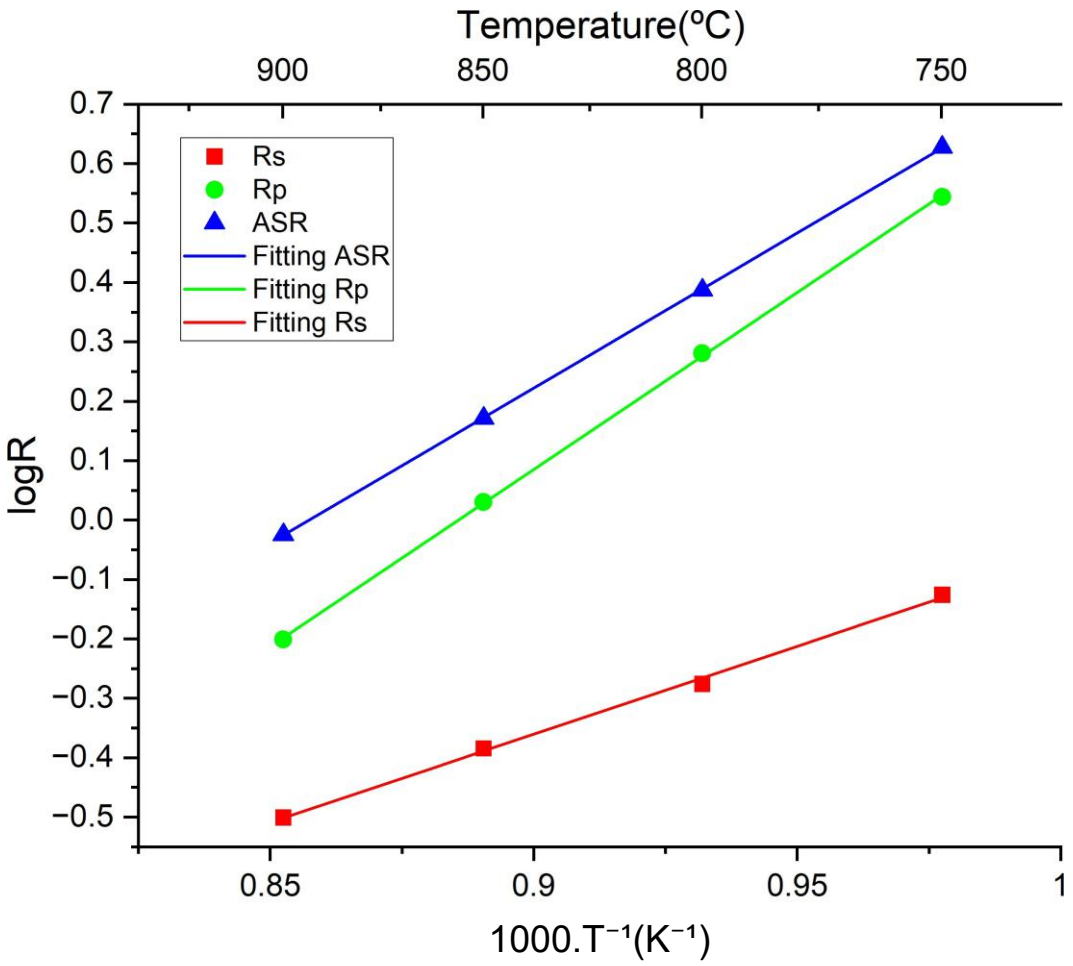

Figure 3.15: Arrhenius plot for HEO-5 SOFC mode

	Temperature (ºC)				Slope	Activation Energy (KJ/mol)
HEO-5 (SOFC)	900	850	800	750		
Rs (Ω)	0.205	0.268	0.344	0.486	2.963	24.634382
Rp (Ω)	0.409	0.696	1.24	2.27	5.96	49.55144
ASR (Ω·cm²)	0.614	0.964	1.584	2.756	5.216	43.365824

Table 3.3: Summary of Rs, Rp, and ASR parameters for HEO-5 in SOFC

After 780 h of operation, four different EIS measurements at 850°C were made to evaluate the impact of changing the cell's fuel and oxidant atmosphere with constant mass flows: 100% H2 / air, 5% H2 / air, 100% H2 / 100% O2, and 5% H2 / 100% O2, as shown in Fig.3.16. Argon was used as a carrier gas for the remaining balance.

The highest recorded voltages were under 100% H2 / 100% O2, indicating faster electrode kinetics and lower polarization losses. This could be explained by enhanced hydrogen oxidation and oxygen reduction rates due to the higher percentage of fuel and oxidant. Conversely, 5% H2 / air showed the lowest voltages, revealing slower reaction

kinetics and higher polarization losses due to limited fuel and oxidant availability.

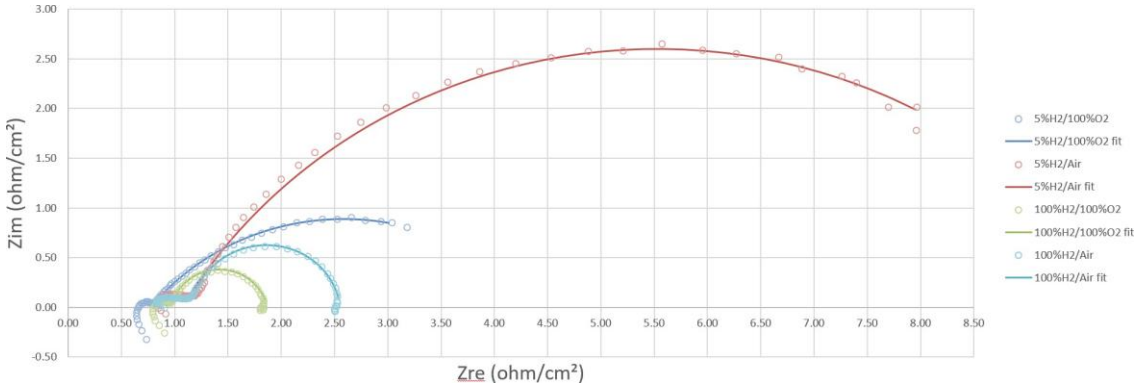

Figure 3.16: Electrochemical Impedance Spectroscopy analysis under different fuel and oxidant compositions for HEO-5 in SOFC

To better understand the results for HEO-5, this cell was compared to a previously studied symmetrical cell using $SrFe_{0.75}M_{0.25}O_3$ (M = Ti or Zr) as the electrode was taken as a reference for the impedance data gathered: at 800ºC, it showed an Rp between 0.5–1.5 $\Omega \cdot cm^2$, compared to a lower value of 1.24 $\Omega \cdot cm^2$ for the studied HEO-5. The reference cell also exhibited an activation energy (Ea) between 1.0–1.2 eV, in contrast to 0.5134 eV for HEO-5 at the same temperature. These results indicate that the previously studied cell had poorer electrode kinetics and higher polarization losses due to its higher Rp, and the higher Ea suggested a stronger temperature dependence for electrochemical reactions [10].

As presented in Fig.3.17, IV curve measurements at the end of the degradation process (at 850ºC) further supported these trends. Before degradation, the electrode displayed low overpotentials and promising performance. After 500 h, higher voltages were required to maintain the same current densities, reflecting degradation effects on the electrode. At a current density of 0.21 A/cm^2, the voltage dropped from approximately 0.89 V to 0.75 V, primarily due to increased polarization resistance. Despite this, the electrode showed relatively stable performance overall. Rs and Rp parameters also change over degradation time, as illustrated in Tab.3.4.

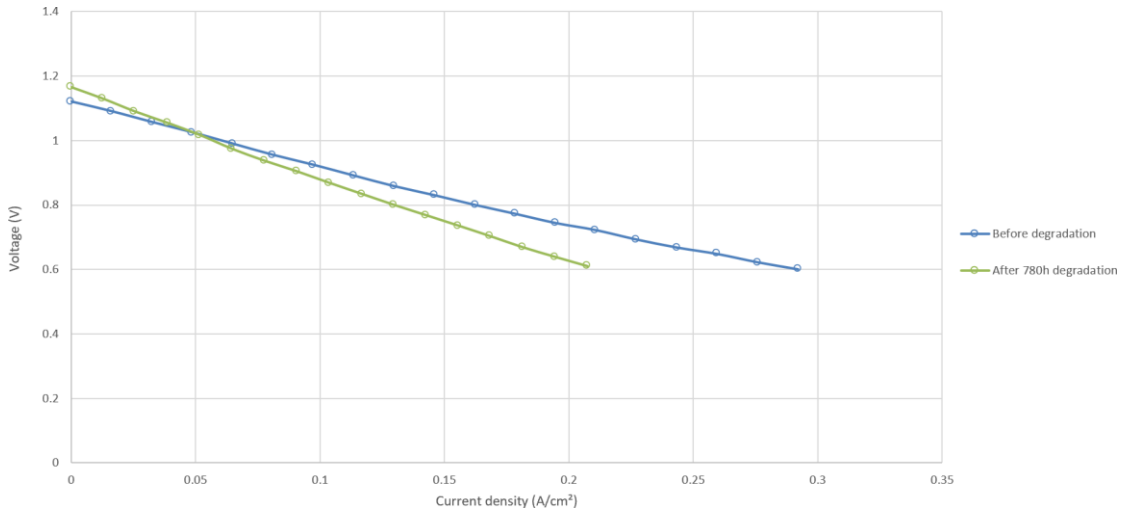

Figure 3.17: Polarization curves before and after degradation for HEO-5 in SOFC mode

HEO-5 (SOFC) before/after deg.	0h	500h	780h
Rs (Ω)	0.268	0.469	0.444
Rp (Ω)	0.696	1.171	1.217

Table 3.4: Summary of Rs and Rp parameters with degradation time

After 780 h of operation, four IV curve measurements were also performed at 850ºC to evaluate the impact of changing the fuel and oxidant atmosphere, under the same previously mentioned conditions and with constant mass flows: 100% H_2 / air, 5% H_2 / air, 100% H_2 / 100% O_2, and 5% H_2 / 100% O_2, as shown in Fig.3.18. Argon was used as the carrier gas.

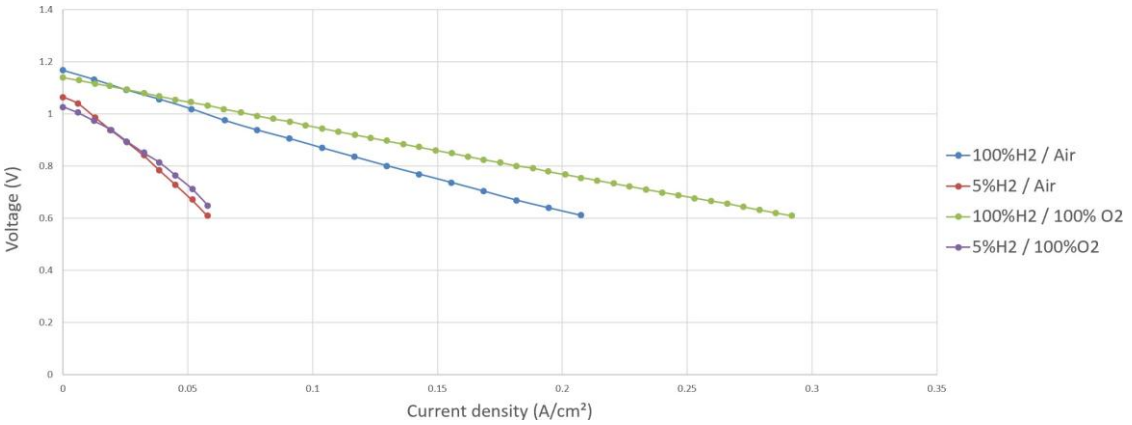

Figure 3.18: Polarization curves under different fuel and oxidant compositions for HEO-5 in SOFC mode

3.4 HEO-7 Anode-Supported Cell

3.4.1 Scanning Electron Microscope

The composition results for HEO-7 were obtained through a XRD analysis. The sample exhibited pronounced and well-defined peaks, indicating a multi-phase and highly crystalline material.

Two main phases were identified. The primary phase corresponded to an orthorhombic crystal structure, prominent between 30º and 70º, matching standard orthorhombic HEO patterns. The most intense peak was observed near 33º, suggesting preferential orientation or a high degree of crystallinity in that direction.

The secondary phase was attributed to a tetragonal structure, observed to a lesser extent. Several minor peaks appeared between 20º-30º and beyond 70º, possibly indicating incomplete homogenization or phase segregation during synthesis or cooling. The presence of this phase may influence electrode performance and stability through properties such as ionic conductivity, depending on its distribution and interfacial compatibility with the primary phase. This analysis is shown in Fig.3.19.

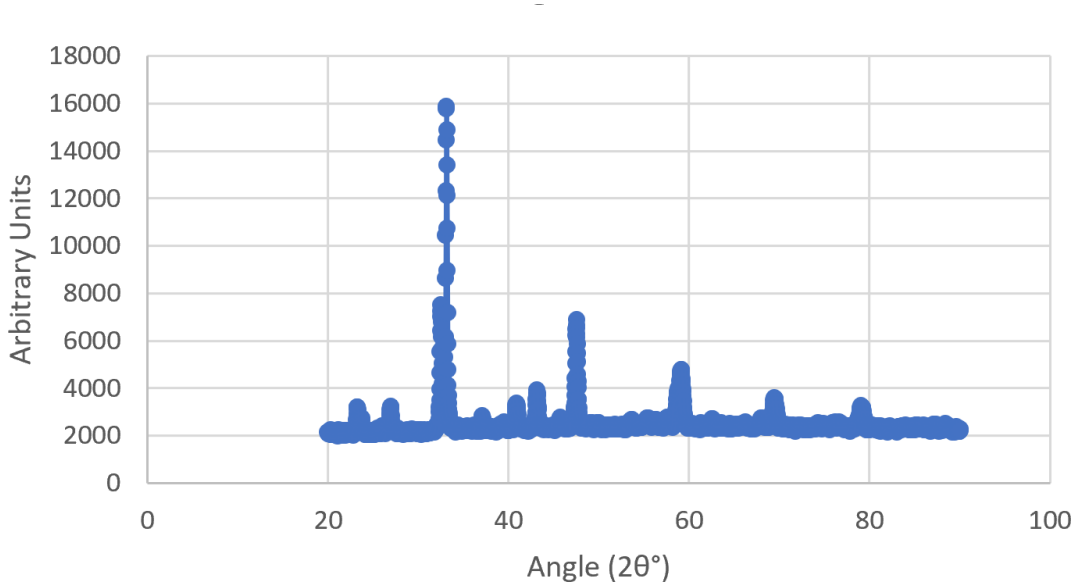

Figure 3.19: X-ray diffraction spectrum for HEO-7

3.5 HEO-7 Anode-Supported Cell in SOEC Mode

3.5.1 Polarization Curves

The IV curve results were measured at different temperatures—900ºC, 850ºC, 800ºC, and 750ºC—and were presented as a function of current density (A/cm^2) versus voltage (V).

As shown in Fig 3.20, measurements showed improved performance at higher temperatures, resulting in smoother curves and lower ohmic and activation losses. In contrast, at lower temperatures, the voltage dropped more rapidly with increasing current density, indicating more pronounced polarization losses. It was concluded that the cell operated more efficiently at higher temperatures, likely due to enhanced ionic conductivity and electrochemical kinetics.

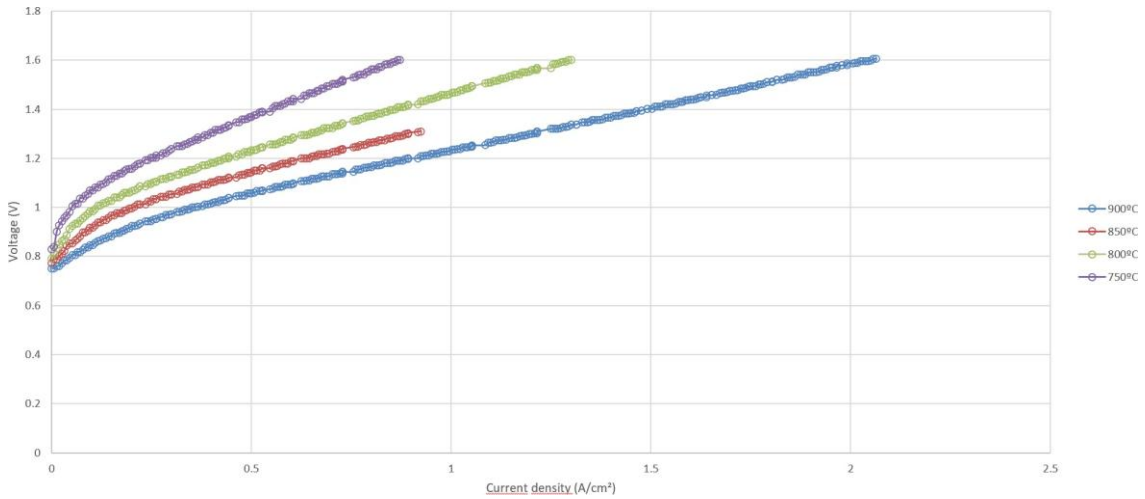

Figure 3.20: Polarization curves for HEO-7 in SOEC mode

To better understand the results for HEO-7, IV curves were compared with the performance of a symmetrical Ni-8YSZ|8YSZ|LSCF (Lanthanum strontium cobalt ferrite (LSCF) = $La_{0.6}Sr_{0.4}Co_{0.2}Fe_{0.8}O_3$) cell at 800ºC. At a current density of 0.25 A/cm^2, the voltage corresponded to 1.15 V, whereas the studied cell at the same current density and temperature showed a similar voltage around 1.10 V, indicating equivalent electrode kinetics and polarization losses under these conditions [47].

3.5.2 Electrochemical Impedance Spectroscopy

EIS measurements were conducted at 1200 mV and at four temperatures: 900ºC, 850ºC, 800ºC, and 750ºC. The results were presented as Nyquist plots, where Real Resistivity (Z', $\Omega \cdot cm^2$) corresponds to electrode resistance, and Imaginary Resistivity (Z'', $\Omega \cdot cm^2$) reflects inductive effects. Fitted curves were included.

As presented in Fig.3.21, the data were modeled using equivalent circuits that included: an inductor in series with four resistors (three in parallel with constant phase elements), an inductor in series with three resistors (two in parallel with constant phase elements) or three resistors in series, each with a parallel constant phase element. One model was chosen over the other depending on the presence of negative Imaginary Resistivity values exhibited in the Nyquist plot, which corresponded to the presence of an inductor or the number of semicircles. exhibited in the Nyquist plot, which corresponded on the number of resistors. In most cases, parameter errors were below 10%.

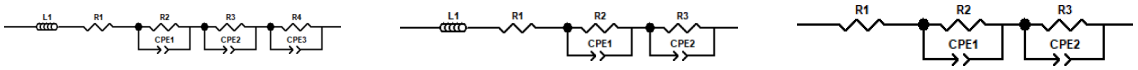

Figure 3.21: Equivalent circuit models for HEO-7 impedance fitting in SOEC mode

The impedance measurements exhibited three depressed arcs corresponding to higher or lower frequencies: the high-frequency arc regards the charge transfer resistance at the interface between the electrolyte and the electrode, the middle-frequency arc corresponds to the reaction kinetics or surface exchange, and the lower-frequency arc to transport processes in the electrode or gas diffusion. These arcs increased in size with decreasing temperature, illustrating better cell performance at higher temperatures due to optimized electrochemical activity and lower polarization losses, as shown in Fig.3.22.

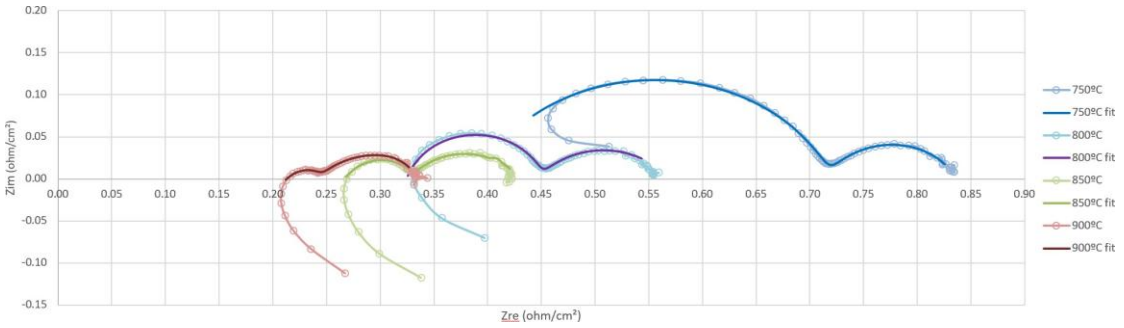

Figure 3.22: Electrochemical Impedance Spectroscopy curves for HEO-7 in SOEC mode at 1200 mV

Arrhenius plots were also constructed to better analyze how Rs, Rp, and ASR parameters evolved under different temperature conditions. The plots displayed three linear fits at the measured temperatures, where Rp, Rs, and ASR exhibited similar slopes. This indicates that temperature influences each component in a comparable manner (electrode polarization, ohmic resistance, and total cell resistance), although Rp showed a slightly steeper slope, suggesting it is marginally more affected by temperature variations, as shown in Fig.3.23. This analysis confirms that resistive processes in the cell are strongly dependent on temperature, highlighting the importance of optimizing cell resistance components to enhance overall performance. A summary table was prepared to better understand the evolution of these parameters with time (Tab.3.5).

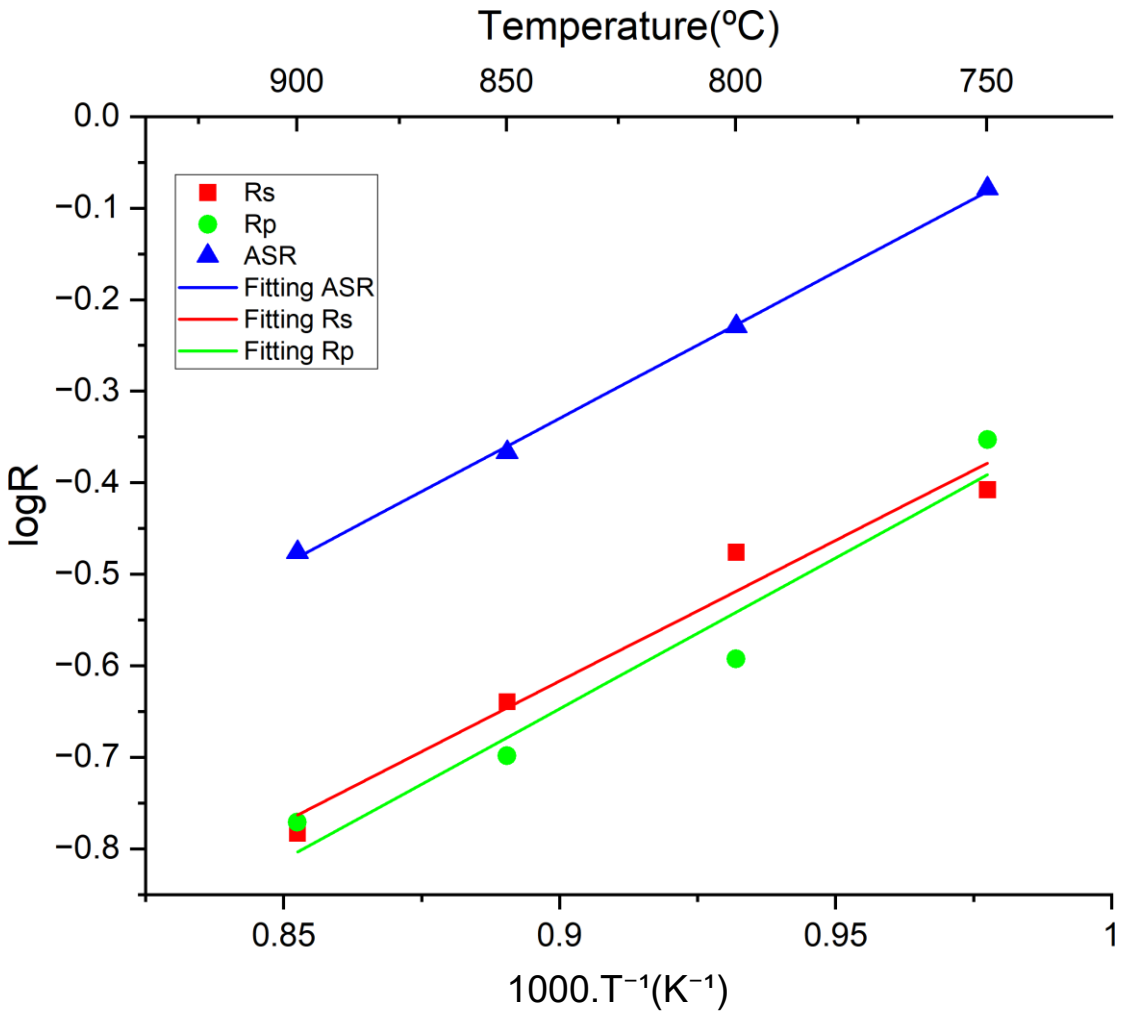

Figure 3.23: Arrhenius plot for HEO-7 in SOEC mode

	Temperature (ºC)				Slope	Activation Energy (KJ/mol)
HEO-7 (SOEC)	900	850	800	750		
Rs (Ω)	0.107	0.149	0.217	0.254	3.074	25.557236
Rp (Ω)	0.11	0.13	0.166	0.288	3.297	27.411258
ASR (Ω·cm²)	0.217	0.279	0.383	0.542	3.197	26.579858

Table 3.5: Summary of Rs, Rp, and ASR parameters for HEO-7 in SOEC

To better understand the results for HEO-7, this cell was compared to a previously studied symmetrical cell using an LSM-YSZ|YSZ|Ni-YSZ configuration (Lanthanum strontium manganite (LSM) = $La_{0.8}Sr_{0.2}MnO_3$) was taken as a reference for the impedance data: at 800ºC, it exhibited an Rp of approximately 0.79 Ω/cm^2, compared to a lower value of 0.166 Ω/cm^2 in the studied cell. The previously studied cell indicated poorer

electrode kinetics and higher polarization losses due to its elevated Rp, while the studied cell demonstrated improved performance under the same conditions through its reduced Rp [48].

3.6 HEO-7 anode-supported cell in SOFC mode

3.6.1 Polarization Curves

The IV curve results were measured at different temperatures: 900ºC, 850ºC, 800ºC, and 750ºC, and were displayed as a function of current density (A/cm^2) versus voltage (V).

As shown in Fig 3.24, measurements showed better performance at higher temperatures, resulting in smoother curves and lower ohmic and activation losses, whereas at lower temperatures, voltage dropped at a faster rate with higher current density corresponding to more pronounced polarization losses. It is believed that the cell demonstrated better efficiency at higher temperatures due to improved ionic conductivity and electrochemical kinetics.

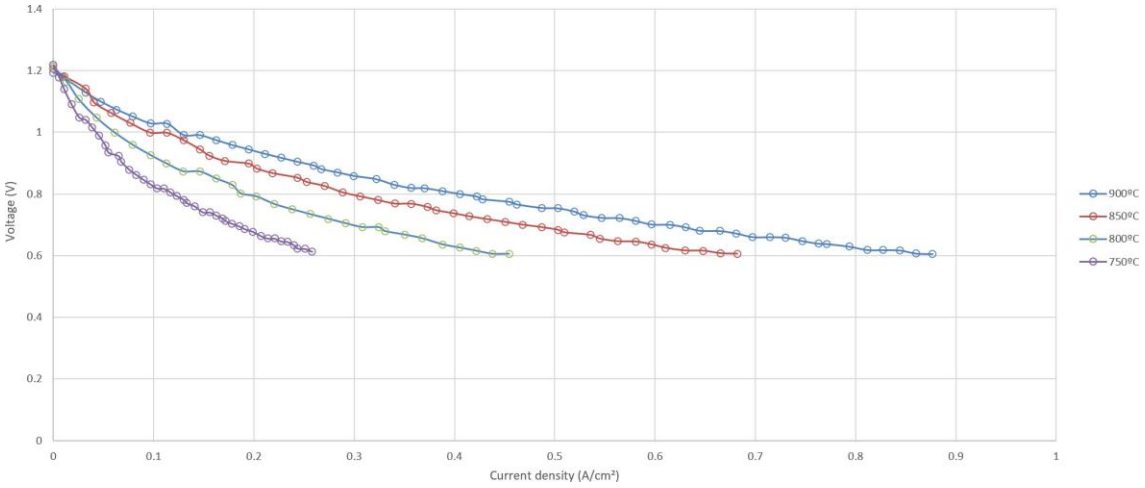

Figure 3.24: Polarization curves for HEO-7 in SOFC mode

To better understand the results for HEO-7, IV curves were compared to the performance of a symmetrical Ni-YSZ|8YSZ|LSM cell at 750ºC. At a current density of 0.25 A/cm^2, it corresponded to a voltage of 0.95 V, whereas the HEO-7 cell at the same current density and temperature corresponded to a voltage around 0.6 V, showing worse electrode kinetics and higher polarization losses under these conditions [49].

3.6.2 Electrochemical Impedance Spectroscopy

The EIS results were analyzed at 700 mV and at measurement temperatures of 900ºC, 850ºC, 800ºC, and 750ºC. These measurements were displayed as Nyquist plots, with Real Resistivity (related to electrode resistivity) as $Z^{'}$ (Ω/cm^2), and Imaginary Resistivity (related to inductance) as $Z^{''}$ (Ω/cm^2), along with their respective fitted curves.

As presented in Fig.3.25, the data were fitted using an equivalent circuit model composed of an inductor in series with four resistors, three of which were parallel with constant phase elements. This model showed parameter errors below 10% in most cases.

An Arrhenius plot was also presented as 1000/T (K^{-1}) versus log(R), where three lines represent electrolyte resistance (Rs), polarization resistance (Rp), and area-specific resistance (ASR) for each temperature analyzed.

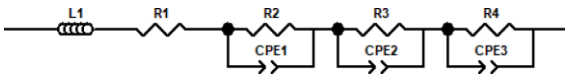

Figure 3.25: Equivalent circuit model for HEO-7 impedance fitting in SOFC mode

The impedance measurements exhibited three depressed arcs corresponding to higher or lower frequencies: the high-frequency arc represents the charge transfer resistance at the interface between the electrolyte and the electrode, the middle-frequency arc corresponds to the reaction kinetics or surface exchange, and the low-frequency arc to transport processes in the electrode or gas diffusion. These arcs increased in size with decreasing temperature, illustrating better cell performance at higher temperatures, such as optimized electrochemical activity and lower polarization losses, as shown in Fig.3.26.

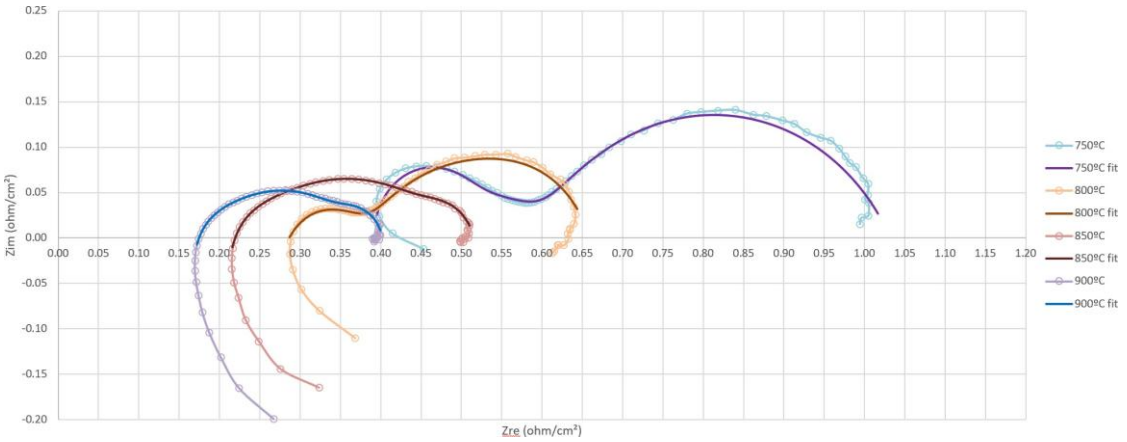

Figure 3.26: Electrochemical Impedance Spectroscopy curves for HEO-7 in SOFC mode at 700mV

Arrhenius plots were also designed to better analyze how Rs, Rp, and ASR parameters change under different temperature conditions. They displayed three linear fits at the measured temperatures, where Rp, Rs, and ASR have similar slopes, indicating that temperature influences each component in a similar way (electrode polarization, ohmic resistance, and total cell resistance). Although Rp has a slightly steeper slope, demonstrating that it is somewhat more affected by temperature variations, as shown in Fig.3.27. This analysis shows that resistive processes in the cell are strongly influenced by temperature, emphasizing the importance of optimizing cell resistance components to enhance cell

performance. A summary table was prepared to better understand the evolution of these parameters with time (Tab.3.6).

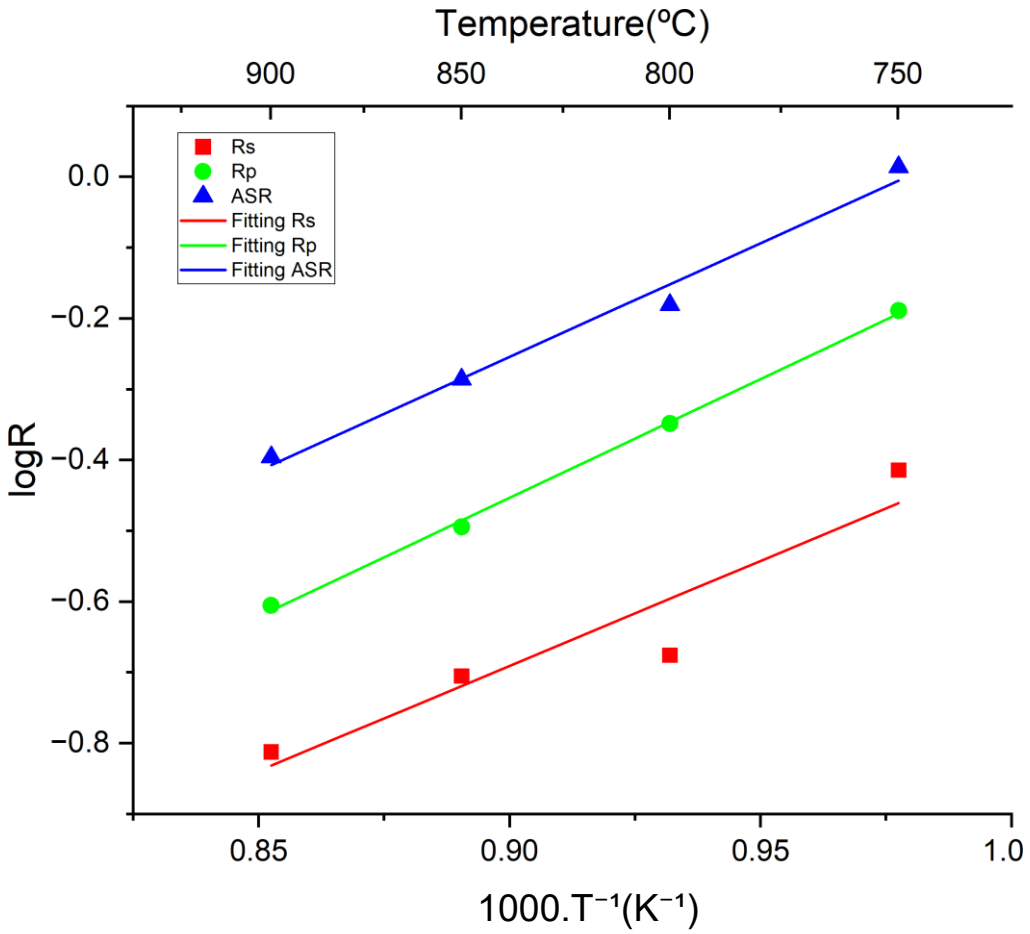

Figure 3.27: Arrhenius plot for HEO-7 in SOFC mode

	Temperature (ºC)				Slope	Activation Energy (KJ/mol)
HEO-7 (SOFC)	900	850	800	750		
Rs (Ω)	0.1	0.128	0.137	0.25	2.967	24.667638
Rp (Ω)	0.161	0.208	0.291	0.42	3.354	27.885156
ASR (Ω·cm²)	0.261	0.336	0.428	0.67	3.215	26.72951

Table 3.6: Summary of Rs, Rp, and ASR parameters for HEO-7 in SOFC

To better understand the results for HEO-7, this cell was compared to a previously studied symmetrical cell using a Ni-8YSZ|8YSZ|LSCF configuration with fuel partial pressures of pH_2 = 0.15 atm and pH_2O = 0.05 atm was taken as a reference for the impedance data: at 800ºC, it showed an Rp around 0.05 Ω/cm^2, compared to a higher value of 0.291 Ω/cm^2 and an Ea of 1.13 eV compared to 0.289 eV for the studied HEO-5 at the same temperature. The previously studied cell indicated much better electrode kinetics

and lower polarization losses due to its lower Rp and at the same time demonstrated a higher Ea, meaning electrochemical reactions improve with increasing temperature [50].

4

Conclusion

After this study, it was concluded that the HEO-5 electrode showed moderately promising results in the different parameters analyzed in both SOEC and SOFC modes, with reasonable Rp/ASR in SOFC, a more stable degradation trend after 400 h, and high stability at low currents in SOEC, although it did not clearly outperform state-of-the-art electrodes. The HEO-7 electrode, on the other hand, the results were poor, failing early and lacking reliable degradation data, which might be ascribed to the poor microstructure.

These electrodes were compared to previously studied ones in similar settings and conditions in order to have an electrode performance reference. Even though these comparisons were legitimate due to their similar characteristics, they cannot be the only performance measurement applied to these electrodes, due to the fact that the previous studies often have different test conditions (temperature, gas composition, current load, electrode composition, etc.). In addition, in the existing literature on symmetrical cells, long-term degradation data are scarce or missing, making direct benchmarking difficult but strengthening the relevance of the present results, since the HEO-5 degradation study provides useful information even if the absolute performance is not yet state-of-the-art:

- **HEO-5 electrode in SOEC mode**: After EIS testing, the HEO-5 electrode exhibited the expected behavior, but when compared to the previously studied cell, the latter still indicated much better electrode kinetics and lower polarization losses due to its lower Rp, and at the same time demonstrated a higher activation energy, meaning that electrochemical reactions improve with greater temperatures. In the IV curve testing, HEO-5 also showed lower performance when compared to the previously studied cell, which indicated better electrode kinetics and lower polarization losses due to its lower voltage. Degradation losses were relatively the same as an equivalent cell, but difficult to interpret due to differences in the current density delivered to the cell [19].

- **HEO-5 electrode in SOFC mode**: After EIS testing, the HEO-5 electrode demonstrated improved performance when compared to the previously studied cell, as the latter indicated much worse electrode kinetics and higher polarization losses

due to its higher Rp, and at the same time demonstrated a higher activation energy, meaning that electrochemical reactions improve with greater temperatures. In IV curve testing, HEO-5 showed comparable electrode kinetics and polarization losses to the previously studied cell, due to the equivalent voltage at the same current density and temperature. Degradation losses were slightly lower in the studied cell, with a quicker stabilization of voltage, but were measured under lower current density, making interpretation difficult [10].

- **HEO-7 electrode in SOEC mode**: After EIS testing, the HEO-7 electrode showed a clear improvement over the previously studied cell, as the latter indicated much worse electrode kinetics and higher polarization losses due to its higher Rp, while the studied cell demonstrated a lower Rp, indicating better performance under the same conditions. In IV curve testing, HEO-7 displayed equivalent electrode kinetics and polarization losses to the previously studied similar cell. Degradation losses were not clearly distinguishable due to comparable performance and limited data on long term operation [47, 48].

- **HEO-7 electrode in SOFC mode**: After EIS testing, the HEO-7 electrode showed lower performance relative to the previously studied cell, as the latter indicated much better electrode kinetics and lower polarization losses due to its lower Rp and at the same time demonstrated a higher activation energy, meaning that electrochemical reactions improve with greater temperatures. In IV curve testing, HEO-7 exhibited worse electrode kinetics and higher polarization losses due to its lower voltage at the same current density and temperature. Degradation losses were not significantly different, though interpretation was limited due to differences in operational conditions [49, 50].

To sum up, the HEO-5 corresponded to the expectations, where it was predicted it would maintain a stable current over a long period of time and would perform at a similar level as other electrodes in electrochemical experiments. The HEO-7 did not correspond to the expectations, where it was thought it would perform even better than the HEO-5 due to the absence of chromium in its composition and so it would not form clusters that could affect its performance. Besides this, it was an electrode that needed microstructural and electrolyte/electrode attachment optimization to really evaluate if it is worth looking deeper into future research.

Future work should focus on testing the HEO-5 electrode under harsher operating conditions, such as CO_2 electrolysis or co-electrolysis, at higher current densities and over extended durations. Microstructure optimization including improved synthesis/sintering, particle size control, porosity tuning, and better electrode/electrolyte attachment would be a crucial step to enhance performance.

Bibliography

[1] D.Sikstrom and V.Thangadurai "A tutorial review on solid oxide fuel cells: fundamentals, materials, and applications". In: Ionics (2020). DOI:10.1007/s11581-024-05824-7. URL: https://doi.org/10.1007/s11581-024-05824-7 (cit. on p. 1).

[2] Y.Tian, N.Abhishek, C.Yang, R.Yang, S.Choi, B.Chi, J.Pu, Y.Ling, J.Irvine and G.Kim "Progress and potential for symmetrical solid oxide electrolysis cells". In: Matter 5 (2025), pp.482–514. DOI:10.1016/j.matt.2021.11.013. URL:https://doi.org/10.1016/j.matt.2021.11.013 (cit. on p. 1).

[3] A. Talukdar, A. Chakrovorty, P. Sarmah, P. Paramasivam, V. Kumar, S. Yadav and S. Manickkam "A Review on Solid Oxide Fuel Cell Technology: An Efficient Energy Conversion System". In: International Journal of Energy Research (2024), vol. 2024, pp. 1–20. DOI:10.1155/2024/6443247. URL: https://doi.org/10.1155/2024/6443247 (cit. on p. 2-7).

[4] C. Su, W. Wang, M. Liu, M. Tadé and Z. Shao, "Progress and Prospects in Symmetrical Solid Oxide Fuel Cells with Two Identical Electrodes". In: *Advanced Energy Materials* (2015), vol. 5, no. 14, pp. 1500188. DOI: 10.1002/aenm.201500188. URL: https://doi.org/10.1002/aenm.201500188 (cit. on p. 2).

[5] A. Tarancón, M. Torrell, F. Baiutti, L. Bernadet, S. Anelli, N. Kostretsova and M. Lira, "Emerging trends in Solid Oxide Electrolysis Cells". In: *Catalonia Institute for Energy Research (IREC)*, SOEC Chapter IREC Final Draft (2024). (cit. on p. 2).

[6] A. Chaisantikulwat, C. Diaz-Goano and E. Meadows, "Dynamic modelling and control of planar anode-supported solid oxide fuel cell". In: *Journal of Power Sources* (2008), vol.176, no. 1, pp. 213–224. DOI: 10.1016/j.compchemeng.2007.12.003. URL: https://doi.org/10.1016/j.compchemeng.2007.12.003 (cit. on p. 2).

[7] A. Kromp, A. Leonide, A. Weber and E. Ivers-Tiffée, "Electrochemical Analysis of Reformate-Fuelled Anode Supported SOFC". In: *Journal of The Electrochemical Society* (2011), vol. 158, no. 8, pp. B980–B990. DOI: 10.1149/1.3597177. URL: https://doi.org/10.1149/1.3597177 (cit. on p. 2).

[8] J. Fergus, "Materials challenges for solid-oxide fuel cells", *JOM*, vol.59 (2007) pp. 56–62. DOI: 10.1007/s11837-007-0153-x. URL: https://doi.org/10.1007/s11837-007-0153-x (cit. on p. 2).

[9] A.Nechache, M. Cassir and A. Ringuedé, "Solid Oxide Electrolysis Cell Analysis by Means of Electrochemical Impedance Spectroscopy: A Review". In: *Journal of PowerSources* (2020), vol. 478, pp.228762. DOI: 10.1016/j.jpowsour.2014.01.110 URL: https://doi.org/10.1016/j.jpowsour.2014.01.110 (cit. on pp. 3–6).

[10] D. Klotz, J. Njodzefon, A. Weber and E. Ivers-Tiffée, "Current-Voltage and Temperature Characteristics of Anode Supported Solid Oxide Electrolyzer Cells (SOEC)". In: *ECS Transactions* (2012), vol. 45, no. 1, pp. 523–530. DOI: 10.1149/1.3701344. URL: https://doi.org/10.1016/10.1149/1.3701344 (cit. on pp. 3, 4, 6, 8, 29, 31, 34, 45).

[11] S. Jiang, "Development of Lanthanum Strontium Manganite Perovskite Cathode Materials of Solid Oxide Fuel Cells: A Review". In: *Journal of Materials Science*, vol. 43, pp. 6799–6833 (2008). DOI:10.1007/s10853-008-2966-6. URL: https://doi.org/10.1007/s10853-008-2966-6 (cit. on pp. 3, 4).

[12] S. Hussain and L. Yangping, "Review of solid oxide fuel cell materials: cathode, anode, and electrolyte". In: *Energy Transitions* (2020), vol. 4, no. 2, pp. 113–126. DOI: 10.1007/s41825-020-00029-8. URL: https://doi.org/10.1007/s41825-020-00029-8 (cit. on p. 3).

[13] P. Kaur and K. Singh, "Cerium oxide-based electrolytes for low- and intermediate-temperature solid oxide fuel cells: state of the art, challenges and future prospects". In: *Sustainable Energy and Fuels* (2025), vol. 9, pp. 3981–3998. DOI: 10.1039/D5SE00526D. URL: https://doi.org/10.1039/D5SE00526D (cit. on pp. 3, 4).

[14] S. Koohfar, M. Ghasemi, T. Hafen, G. Dimitrakopoulos, D. Kim, J. Pike, S. Elangovan, E. Gomez and B. Yildiz, "Improvement of oxygen reduction activity and stability on a perovskite oxide surface by electrochemical potential". In: *Nature Communications* (2023), vol. 14, no. 1, pp. 42462. DOI: 10.1038/s41467-023-42462-5. URL: https://doi.org/10.1038/s41467-023-42462-5 (cit. on pp. 3, 4).

[15] W. Li, Y. Cheng, Q. Zhou, T. Wei, Z. Li, H. Yan, Z. Wang and X. Han, "Evaluation of double perovskite Sr_2FeTiO_6–δ as potential cathode or anode materials for intermediate-temperature solid oxide fuel cells". In: *Journal of Power Sources* (2015), vol. 41, pp. 12393–12400. DOI: 10.1016/j.ceramint.2015.06.074. URL: https://doi.org/10.1016/j.ceramint.2015.06.074 (cit. on p. 3).

[16] F. Han, Z. Wang, S. Zhang, C. Li and S. Barnett, "Highly efficient perovskite-based fuel electrodes for solid oxide electrochemical cells via in-situ nanoparticle exsolution and electron conduction enhancement". In: *Journal of Power Sources* (2025), vol. 580, pp. 240–250. DOI: 10.1016/j.apcatb.2024.124676. URL: https://doi.org/10.1016/j.apcatb.2024.124676 (cit. on p. 3).

[17] X. Zhang, C. Wang, K. Liu, Y. Zhou, Z. Huang, T. Chen, G. Zhang, N. Sun, Z. Zhuang, L. Xu and S. Wang, "Significantly enhanced stability and activity of a perovskite oxygen electrode for reversible protonic ceramic electrochemical cells by heterointerface engineering". In: *Journal of Advanced Ceramics* (2025), vol. 14, no 7,pp.9221108.DOI:10.26599/JAC.2025.9221108.URL:https://doi.org/10.26599/JAC.2025.9221108 (cit. on pp. 3, 5).

[18] S. Singhal and K. Kendall, "High-temperature solid oxide fuel cells: Fundamentals, design and applications". In: *Elsevier* (2003). DOI: 10.1016/B978-1-85617-387-2.X5016-8. URL: https://doi.org/10.1016/B978-1-85617-387-2.X5016-8 (cit. on p. 4).

[19] D. Le, H. Nguyen, S. Yu, H. Le and T. Hoang, "Progress and outlook of solid oxide fuel cell technology for stationary power generation applications". In: *Frontiers in Energy Research* (2003), vol. 13. DOI: 10.3389/fenrg.2025.1650696. URL: https://doi.org/10.3389/fenrg.2025.1650696 (cit. on pp. 4–6, 25, 27, 28, 44).

[20] S. Skinner and M. Laguna-Bercero, "Advanced Inorganic Materials for Solid Oxide Fuel Cells". In: *Journal of Materials Science* (2011), vol. 2. DOI: 10.1002/9780470977798.ch2. URL: https://doi.org/10.1002/9780470977798.ch2 (cit. on p. 4).

[21] M. Harashid, R. Chen, S. Ahmad, A. Ismail and N. Baharuddin, "Recent advances in electrode material for symmetrical solid oxide fuel cells and way forward sustainability based on local mineral resources". In: *International Journal of Energy Research* (2022), vol. 46, pp. 22188–22221. DOI: 10.1002/er.8579. URL: https://doi.org/10.1002/er.8579 (cit. on p. 4).

[22] C. Rost, E. Sachet, T. Borman, A. Moballegh, E. Dickey, D. Hou, J. Jones, S. Curtarolo and J. Maria, "Entropy-stabilized oxides". In: *Nature Communications* (2015), vol. 6, pp. 8485. DOI: 10.1038/ncomms9485. URL: https://doi.org/10.1038/ncomms9485(cit. on p. 4).

[23] D. Miracle and O. Senkov, "A critical review of high-entropy alloys and related concepts". In: *Acta Materialia* (2017), vol. 122, pp. 448–511. DOI: 10.1016/j.actamat.2016.08.081. URL: https://doi.org/10.1016/j.actamat.2016.08.081 (cit. on pp. 4, 5).

[24] M.Gao, Y.Zhang and P.Liaw, "High-entropy alloys: Fundamentals and applications". In: *Springer* (2016). DOI: 10.1007/978-3-319-27013-5. URL: https://doi.org/10.1007/978-3-319-27013-5 (cit. on p. 4).

[25] M. Ghassemi, M. Kamvar and R.S-Wilckens, "Classification of solid oxide fuel cells". In: *Academic Press* (2020), vol. 10, pp. 17–46. DOI: 10.1016/B978-0-12-815753-4.00002-6.URL:https://doi.org/10.1016/B978-0-12-815753-4.00002-6 (cit.on p.5).

[26] H. Li, W. Wei, F. Liu, X. Xu, Z. Li and Z. Liu, "Identification of internal polarization dynamics for solid oxide fuel cells investigated by electrochemical impedance spectroscopy and distribution of relaxation times". In: *Elsevier* (2023), vol. 267, pp. 126482. DOI: 10.1016/j.energy.2022.126482. URL: https://doi.org/10.1016/j.energy.2022.126482 (cit. on p. 5).

[27] M.Sohal, "Degradation in Solid Oxide Cells During High Temperature Electrolysis". In: *Idaho National Laboratory* (2009). DOI: 10.2172/957533 URL: https://doi.org/10.2172/957533 (cit. on pp. 5–9).

[28] H. Xu, K. Cheng, M. Chen, L. Zhang, K. Brodersen and Y. Du, "Interdiffusion between gadolinia doped ceria and yttria stabilized zirconia in solid oxide fuel cells: Experimental investigation and kinetic modeling". In: *arXiv* (2019). DOI: 10.48550/arXiv.1910.11947. URL: https://doi.org/10.48550/arXiv.1910.11947 (cit. on p. 6).

[29] A. Amiri and R. Shahbazian-Yassar, "Recent progress of high-entropy materials for energy storage and conversion". In: *Advanced Materials* (2021), vol. 9. DOI: 10.1039/D0TA09578H. URL: https://doi.org/10.1039/D0TA09578H (cit. on p. 6).

[30] K. Zheng, J. Lach, P. Czaja, M. Gogacz, P. Czach, A. Brzoza-Kos, P. Winiarz and J. Luo, "Designing high-performance quasi-symmetrical solid oxide cells with a facile chemical modification strategy for Sr_2Fe_2−xWxO_6−δ ferrites electrodes with in situ exsolution of nanoparticles". In: *Journal of Power Sources* (2023), vol. 587, pp. 233707.DOI:10.1016/j.jpowsour.2023.233707.URL:https://doi.org/10.1016/j.jpowsour.2023.233707 (cit. on p. 6).

[31] C. Yao, W. Liu, H. Zhang, H. Wang, W. Zhang, X. Lang and K. Cai, "High-entropy perovskite ($Pr_{1/6}Nd_{1/6}Sm_{1/6}Ba_{1/6}Sr_{1/6})_{6/7}(Mn_{1/6}Co)_{6/7}O_3$-δ as a highly active and CO_2 durable cathode for solid oxide fuel cells". In: *Applied Catalysis B: Environment and Energy* (2025), vol. 363, no. 15, pp. 124789. DOI: 10.1016/j.apcatb.2024.124789. URL: https://doi.org/10.1016/j.apcatb.2024.124789 (cit. on pp. 6, 7).

[32] M. Zhang, Z. Du, Y. Zhang and H. Zhao, "Progress of Perovskites as Electrodes for Symmetrical Solid Oxide Fuel Cells". In: *ACS Applied Energy Materials* (2022), vol. 11, pp. 13081–13095. DOI:10.1021/acsaem.2c02149. URL: https://doi.org/10.1021/acsaem.2c02149 (cit. on p. 6).

[33] A. Voskanyan, K. Lilova, S. McCormack, W. Kriven and A. Navrotsky, "A new class of entropy stabilized oxides: Commensurately modulated $A_6B_2O_{17}$ (A = Zr, Hf; B = Nb, Ta) structures". In: *Scripta Materialia* (2021), vol. 204, pp. 114139. DOI: 10.1016/j.scriptamat.2021.114139.URL:https://doi.org/10.1016/j.scriptamat.2021.114139 (cit. on p. 6).

[34] M. Tsai and J. Yeh, "High-Entropy Alloys: A Critical Review". In: *Taylor and Francis* (2014), vol. 2, no. 3, pp. 107–123. DOI: 10.1080/21663831.2014.912690. URL: https://doi.org/10.1080/21663831.2014.912690 (cit. on p. 7).

[35] S. Rajendrachari, "Handbook of High Entropy Alloys: Fundamentals to Applications". In: *CRC Press* (2025), pp. 460. DOI: 10.1201/9781003664093. URL: https://doi.org/10.1201/9781003664093 (cit. on p. 7).

[36] A. Sarkar, L. Velasco, D. Wang, Q. Wang, G. Talasila, L. Biasi, C. Kübel, T. Brezesinski, S. Bhattacharya, H. Hahn and B. Breitung, "High entropy oxides for reversible energy storage". In: *Nature Communications* (2018), vol. 9, no. 3400. DOI: 10.1038/s41467-018-05774-5. URL: https://doi.org/10.1038/s41467-018-05774-5 (cit. on p. 7).

[37] Z. Sun, Y. Zhao, C. Sun, Q. Ni, C. Wang and H. Jin, "High entropy spinel-structure oxide for electrochemical application". In: *Chemical Engineering Journal* (2022), vol. 431, pp.133448. DOI:10.1016/j.cej.2021.133448. URL: https://doi.org/10.1016/j.cej.2021.133448 (cit. on pp. 8, 9).

[38] J. Li, Q. Cai and B. Horri, "Highly conductive and stable electrolytes for solid oxide electrolysis and fuel cells: fabrication, characterisation, recent progress and challenges". In: *Materials Advances* (2025), vol. 6, pp. 39-83. DOI: 10.1039/D4MA00690A. URL: http://dx.doi.org/10.1039/D4MA00690A (cit. on p. 8).

[39] M. Lang, C. Bohn, K. Couturier, X. Sun, S. McPhail, T. Malkow, A. Pilenga, Q. Fu and Q. Liu, "Electrochemical Quality Assurance of Solid Oxide Electrolyser (SOEC) Stacks". In: Journal of the Electrochemical Society (2023), vol. 166, no. 15, pp. F1180. DOI: 10.1149/2.0041915jes. URL: https://doi.org/10.1149/2.0041915jes (cit. on p. 8).

[40] X. Chen and Y. Wang, "Solid-State Electrochemistry and Solid Oxide Fuel Cells: Status and Future Prospects". In: *Electrochemical Energy Reviews* (2022), vol. 5, no. 21, pp.2520–8136. DOI:10.1007/s41918-022-00160-8. URL: https://doi.org/10.1007/s41918-022-00160-8 (cit. on p. 8).

[41] J. Fergus, R. Hui, X. Li, D. Wilkinson and J. Zhang, "Solid Oxide Fuel Cells". In: *CRC Press* (2009), pp.298. DOI:10.1201/9781420088847. URL: https://doi.org/10.1201/9781420088847 (cit. on p. 8).

[42] W. Zhang and Y. Hu, "Material design and performance of carbon monoxide-fueled solid oxide fuel cells: A review", *Energy Science and Engineering* (2023), vol.11, pp.3276–3288. DOI:10.1002/ese3.1502. URL: https://doi.org/10.1002/ese3.1502 (cit. on pp. 8, 9).

[43] H. Seo, A. Staerz, G. Dimitrakopoulos, D. Kim, B. Yildiz and H. Tuller, "Degradation and recovery of solid oxide fuel cell performance by control of cathode surface acidity: Case study—Impact of Cr followed by Ca infiltration". In: *Journal of Power Sources* (2023), vol.558 pp.232589. DOI: 10.1016/j.jpowsour.2022.232589.URL:https://doi.org/10.1016/j.jpowsour.2022.232589 (cit. on p. 9).

[44] H. Kim, J. Mason, W. Epting, H. Abernathy, A. Rollett and P. Salvador, "Systematic and predictive trends to chromium poisoning in solid oxide fuel cell cathodes". In: Journal *of Power Sources* (2024), vol.603 pp.234390. DOI: 10.1016/j.jpowsour.2024.234390.URL:https://doi.org/10.1016/j.jpowsour.2024.234390 (cit. on p. 9).

[45] L. Omeiza, A. Kabyshev, K. Bekmyrza, K. Kuterbekov, M. Kubenova, Z. Zhumadilova, Y. Subramanian, M. Ali, N. Aidarbekov and A. Azad, "Constraints in sustainable electrode materials development for solid oxide fuel cell: A brief review". In: *Materials Science for Energy Technologies* (2025), vol.8 pp.32–43. DOI: 10.1016/j.mset.2024.07.001. URL: https://doi.org/10.1016/j.mset.2024.07.001 (cit. on p. 9).

[46] H. Yuan, H. Dai, P. Ming, W. Xueyuan and X. Wei, "Quantitative analysis of internal polarization dynamics for polymer electrolyte membrane fuel cell by distribution of relaxation times of impedance". In: *Applied Energy* (2021), vol.303 pp.117640.DOI:10.1016/J.APENERGY.2021.117640.URL:https://doi.org/10.1016/J.APENERGY.2021.117640 (cit. on p. 9).

[47] R. Xu, S. Liu, M. Yang, G. Yang, Z. Luo, R. Ran, W. Zhou and Z. Shao, "Advancements and prospects of perovskite-based fuel electrodes in solid oxide cells for CO_2 electrolysis to CO". In: *Chemical Science* (2024), vol.15, pp.11166–11187. DOI: 10.1039/D4SC03306J. URL: http://dx.doi.org/10.1039/D4SC03306J (cit. on pp. 37, 45).

[48] X. Luo, A. Wu, J. Sang, N. Huang, B. Han, C. Wang, Y. Gao, W. Guan and S. Singhal, "The properties of the fuel electrode of solid oxide cells under simulated seawater electrolysis". In: *International Journal of Hydrogen Energy* (2023), vol.48 pp.10359–10367. DOI:10.1016/j.ijhydene.2022.11.350. URL: https://doi.org/10.1016/j.ijhydene.2022.11.350 (cit. on pp. 40, 45).

[49] R. Jacobs, T. Mayeshiba, J. Booske and D. Morgan, "Material discovery and design principles for stable, high activity perovskite cathodes for solid oxide fuel cells". In: *Advanced* (2018), vol.8 pp.1702708. DOI: 10.1002/aenm.201702708. URL: https://doi.org/10.1002/aenm.201702708 (cit. on pp. 40, 45).

[50] J. Fergus, “Lanthanum chromite-based materials for solid oxide fuel cell interconnects”. In: *Solid State Ionics* (2004), vol.171 pp.1–15. DOI: 10.1016/j.ssi.2004.04.010. URL: https://doi.org/10.1016/j.ssi.2004.04.010 (cit. on pp. 43, 45).